2025-04

Stapp Car Crash Journal, Vol. 69, pp. 82-113

Investigation of Injury Risk Functions of THOR-AV 50th Percentile Male Dummy

Z. Jerry Wang, George Hu
Humanetics Innovative Solutions, Inc.

ABSTRACT – This research investigated injury risk functions (IRF) for the THOR-AV 50th percentile male dummy in accordance with ISO TS18506, focusing on areas with design changes. The IRF development utilized a combination of physical tests and finite element (FE) model simulations. For certain postmortem human subject test cases lacking physical dummy tests, the validated Humanetics THOR-AV FE model (v0.7.2) was used to quickly generate data, with the understanding that final IRFs based on full physical test data might offer greater accuracy. Log-logistic, log-normal, and Weibull survival functions were fitted with 95% confidence intervals. The Akaike Information Criterion, Goodman-Kruskal-Gamma, Area under the Curve of Receiver Operating Characteristic, and Quantile-Quantile plot were employed to assess the prediction strength and relative quality of the final IRF selections. Among the three survival distributions, the Weibull distribution provided the best fit. The lumbar Fz was identified as the best indicator for lumbar spine injury, followed by Lij. The Fz injury risk values at 5%, 25%, and 50% probabilities are 2170N, 3560N, and 4856N for MAIS2+, respectively. The Lij injury risk values at 5%, 25%, and 50% probabilities are 0.44, 0.65, and 0.79 for MAIS2+, respectively. Abdomen pressure from APTS sensors was found to be a weak indicator for abdomen injury prediction, with injury risk values at 5%, 25%, and 50% probabilities being 128, 209, and 268 kPa for MAIS2+, respectively. The total ASIS force from the left and right ASIS load cells was a better injury predictor than the maximum ASIS load from the individual load cells, with injury risk values at 5%, 25%, and 50% probabilities being 542, 1872, and 3522 Newtons for MAIS2+, respectively.

KEYWORDS – dummy, frontal, injury risk function, reclined, THOR-AV.

INTRODUCTION

With advancements in technology over the past decade, Automated Driving System (ADS) equipped vehicles have become increasingly popular. As driving duties are alleviated, vehicle occupants may adopt various seating postures (Jorlöv et al. 2017, Kitagawa et al. 2017). One common posture is reclining, particularly for resting during long journeys. However, current occupant safety standards only require traditional upright seating postures, with a seatback angle of 25°. Studies have shown that the commonly used belt system integrated into the B-pillar poses higher injury risks for occupants in a reclined seating posture (Mishra et al. 2024). The National Highway Traffic Safety Administration (NHTSA) has demonstrated that the Test device for Human Occupant Restraint (THOR) dummy cannot be configured to represent a reclined occupant without modifications (Prasad 2019). Therefore, an anthropomorphic test device (ATD) is necessary to evaluate the effectiveness of restraint systems in both upright and reclined seating positions.

To address the need for assessing restraint systems for reclined occupant safety, the THOR-AV, a modified THOR crash test dummy, was developed to extend THOR's capabilities to reclined seating postures. The THOR-AV features a new neck design that is simpler than the THOR neck but offers better biofidelity compared to both the THOR and Hybrid III 50th neck (Wang et al. 2021). The lumbar spine of the THOR-AV was redesigned with a circular cross-section (as opposed to the rectangular cross-section of the THOR lumbar) and is longer to more closely match the human lumbar length. The pelvic bone was redesigned to align with the latest human pelvis bone geometry defined by Reed et al. (2013). The THOR-AV

Address correspondence to: Dr. Z.J. Wang, 23300 Haggerty Rd, Farmington Hills, MI 48335, USA. Electronic mail: jwang@humaneticsgroup.com

abdomen is equipped with abdomen pressure twin sensors (APTS), which replaced the abdomen Infra-red telescope rod for assessment of chest compression (IR-TRACC) devices. The THOR-AV was designed to represent occupants in reclined seating postures up to 60° (extended from the THOR standard seating posture with a 25° seatback angle) according to the volunteer regression model developed by Reed et al. (2019). The details of the lumbar, pelvic bone, and pelvis flesh designs were documented in Wang et al. (2022a and 2022c).

The THOR-AV dummy underwent extensive evaluation in various sled test conditions to assess its biofidelity against Postmortem Human Subject (PMHS) corridors (Wang et al. 2022a, 2022b) using the NHTSA BioRank method (Rhule et al. 2018 and Hagedorn et al. 2022), demonstrating good to excellent biofidelity. Additionally, the THOR-AV was tested under rearward-facing frontal crash pulse conditions, showing good biofidelity and durability (Wang 2022c). The dummy was also utilized in an accident reconstruction test (Ostermaier et al. 2020) and in zero-gravity-seat (NASA 2013) testing to evaluate its suitability and durability in reclined seating postures.

Given the THOR-AV's demonstrated good to excellent biofidelity (Wang et al. 2022a, 2022b, and 2022c) and its proven durability through various tests, it became necessary to develop injury risk functions (IRF) to quantitatively assess occupant injury risks associated with restraint systems. The modifications to the THOR dummy focused on enhancing the neck, abdomen, lumbar, and pelvis designs. With the THOR injury criteria already published by NHTSA, this research will concentrate on the areas where design changes were made, specifically the lumbar spine, abdomen, pelvis, and neck. For other regions, the authors recommend using the NHTSA injury criteria, as the THOR-AV shares the same design as the THOR in those areas, such as the head, chest, and lower extremities (Craig et al. 2020).

Over the past few decades, various statistical methods have been employed to develop injury risk curves. Mertz et al. (1996) used a certainty method, while Kuppa et al. (2003) utilized logistic regression. Kent et al. (2004) applied survival analysis with a Weibull distribution. Nusholtz et al. (1999) and Di Domenico et al. (2005) used the consistent threshold estimate (CTE). Petitjean et al. (2009) developed injury risk curves for the WorldSID 50th male dummy under the framework of the International Organization for Standardization / Subcommittee12 / Technical Committee 22 / Working Group 6 (ISO/SC12/TC22/WG6), comparing results from various numerical methods, including Mertz/Weber, CTE, survival analysis, and logistic regression. Petitjean et al. (2011) evaluated these methods for constructing injury risk curves, forming the basis of the ISO technical specification documented in ISO TS18506.

The objective of this research is to develop injury risk functions for the THOR-AV dummy, focusing on the body segments with design changes made to the THOR-50M dummy, specifically in the abdomen, lumbar spine, and pelvic bone. Although the THOR-AV also features a new neck design, the investigation of neck injury risk functions is not included in this study and is planned for future publication.

METHODS

THOR-AV Testing and Simulation with FE model

THOR-AV was tested in many different conditions, including data published in Wang et al. (2021, 2022a, 2022b, 2022c). Additionally, the THOR-AV has been tested in the University of Michigan Transportation Research Institute (UMTRI) 50 km/h, Richardson et al. 2020, and Guettler et al. 2023 test conditions by the same test labs that conducted the PMHS tests. Information on these tests will be published at a later date. For test conditions where the THOR-AV was not physically tested but selected for injury risk function investigation, results from finite element simulations using the THOR-AV FE model (v0.7.2) were utilized. It is understood that ultimately, physical tests of the THOR-AV are necessary to update the injury risk functions for improved accuracy.

In this study, two different abdomen designs were utilized: one for the upright posture and another for the reclined seat. The reclined abdomen includes an extension from the upright design to fill the gap between the ribcage and the top of the abdomen created by the reclined dummy configuration, as illustrated in Figure 1.

The THOR-AV FE model (v0.7.2) was used for simulations in this study, incorporating all meshes and material properties from the Humanetics THOR FE model (v1.8.1) for shared parts. Additional validations were conducted for the redesigned parts unique to THOR-AV. These tests included neck tests (flexion, lateral bending, oblique bending, and torsion, with all test data in Wang et al. 2021), impact tests of the APTS pressure sensor at low and high speeds, a sled test of the lumbar spine at two different speeds (4 and 6.4 m/s) with and without offset mass (twist), pelvis buttock impact tests, upper and lower thorax impact tests (4.3 m/s), upper abdomen steering wheel impact

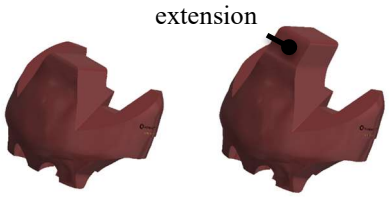

Figure 1. THOR-AV abdomen, design for upright posture (left side), design for reclined posture (right side)

tests, lower abdomen rigid bar tests, and a sled test according to Richardson et al. (2020a). The details of the validation were documented in the Humanetics THOR-AV 50M dummy FE model technical report and user's manual (Humanetics 2024). Generally, the correlation between the results of the THOR-AV FE model (v0.7.2) and physical tests had a CORA score (Gehre et al. 2009) higher than 0.80 for the compared data channels. The peak values of the related data channels from the validation test data and FE results are summarized in Appendix 2 for reference.

Survival Function Fits

In this study, the ISO TS18506 technical specification was followed for IRF development. The technical specification outlines ten steps:

1. Collect the relevant data
2. Assign the censoring status
3. Check for a single injury mechanism
4. Estimate the coefficients
5. Identify overly influential observations ("dfbeta" was used for this purpose)
6. Check the distribution assumption
7. Choose the best distribution
8. Check the validity of the prediction
9. Calculate 95% confidence intervals and their relative size
10. Determine the quality index

The following sections describe the process for injury risk function development for each body segment. The cumulative density functions (CDF) for log-logistic, log-normal, and Weibull distributions used in this study are summarized in equations (1), (2), and (3).

Loglogistic CDF:

$$P(x,\alpha,\beta) = \frac{1}{1+\left(\frac{x}{\alpha}\right)^{-\beta}} \quad (1)$$

Lognormal CDF:

$$P(x) = \frac{1}{2}\left[1+\operatorname{erf}\left(\frac{lnx-\mu}{\sigma\sqrt{2}}\right)\right] \quad (2)$$

Weibull CDF:

$$P(x,\alpha,\beta) = \begin{cases} 1-e^{-\left(\frac{x}{\alpha}\right)^{\beta}}, & x \geq 0 \\ 0, & x < 0 \end{cases} \quad (3)$$

RStudio 2024.09.0 Build 375 (Posit Software, PBC) with R version 4.4.1 (2024-06-14 ucrt, The R Foundation for Statistical Computing, Platform: x86_64_w64_mingw32/x64) was used to develop R codes to process the data according to the steps outlined above.

Akaike Information Criterion (AIC), Goodman Kruskal Gamma (GKG), Area under the Curve of Receiver Operating Characteristic (AUROC), and Quality Index at 50% injury risk values were provided to evaluate the quality of the survival fits.

Data Censoring

The non-injurious cases were categorized as right censored. For the injurious cases, the maximum values were used for the survival fit when the time of injury was not known. If the time of injury was not reported, the injurious cases were treated as left censored. For abdomen pressure, when the data was treated as left-censored, the survival fit did not converge. Therefore, these cases were treated as exact in the survival analysis.

Scaling Method

PMHS test data were used to guide ATD designs by providing target biomechanical responses. However, PMHS specimens vary widely due to limited availability for biomechanical research. To address response differences due to anthropometry, normalization was typically employed. Eppinger et al. (1984) introduced mass-based normalization. Mertz (1984) developed a procedure to estimate the response characteristics of a standard subject based on the measured responses of subjects with different physical characteristics, a method also used by Viano (1989). Moorhouse (2013) proposed an improved procedure using the effective stiffness of the subject derived from response data, rather than calculating it from characteristic length, assuming constant modulus and geometric similitude within the impacted body region.

In this study, most of the PMHS tests selected for developing injury risk functions are sled tests, which generally did not provide data to evaluate subject responses using the enhanced method proposed by

Moorhouse (2013). Therefore, the mass-based normalization methods by Eppinger et al. (1984) were utilized. For each load case, the ATD test data were scaled to the corresponding PMHS case, and these scaled values, paired with the corresponding PMHS AIS scores, were used to develop the injury risk function (Petitjean et al. 2009).

The THOR-AV 50M was designed to represent a 50th percentile male, with a mass of 76 kg and a stature of 175 cm. These values are used in the scaling calculations for M_{ATD} and L_{ATD}, respectively.

The following formulas were used for scaling in this study.

Mass scaling ratio

$$\lambda_m = \frac{M_{PMHS}}{M_{ATD}} \quad (5)$$

Stiffness scaling ratio

$$\lambda_k = \frac{D_{PMHS}}{D_{ATD}} \quad (6)$$

Force scaling ratio

$$\lambda_F = \sqrt{\lambda_m \lambda_k} \quad (7)$$

Moment scaling ratio

$$\lambda_{mo} = \frac{MO_{PMHS}}{MO_{ATD}} = \frac{F_{PMHS} * L_{PMHS}}{F_{ATD} * L_{ATD}} = \sqrt{\lambda_m \lambda_k} * \lambda_L \quad (8)$$

Abdomen pressure scaling ratio:

$$\lambda_p = \frac{p_{PMHS}}{p_{ATD}} = \frac{\frac{F_{PMHS}}{A_{PMHS}}}{\frac{F_{ATD}}{A_{ATD}}} = \left(\frac{F_{PMHS}}{F_{ATD}}\right) * \left(\frac{A_{ATD}}{A_{PMHS}}\right) = \sqrt{\lambda_m \lambda_k}/\lambda_L^2 \quad (9)$$

Where D represents the depth, L represents the stature, p represents the pressure, F represents the force, M represents the mass, MO represents the moment.

When scaling the THOR-AV abdomen pressure data to its respective PMHS specimen, if abdomen depth information was not available, the abdomen circumference was used. In the cases from Guettler et al. (2023), where both abdomen depth and circumference were not reported, a linear regression fit of the abdomen depth and body mass/stature/BMI from the available PMHS specimens was investigated to determine the best method for estimating abdomen depth. The linear regression fit with BMI had the highest R^2 value of 0.3154 and was applied to the Guettler et al. (2023) abdomen data, although the R^2 value does not indicate a strong relationship between abdomen depth and BMI. The linear regression fits are shown in Figure 2 through Figure 4.

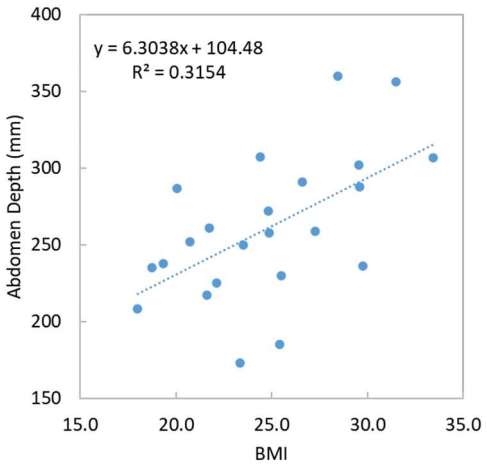

Figure 2. Linear regression fit of abdomen depth and BMI

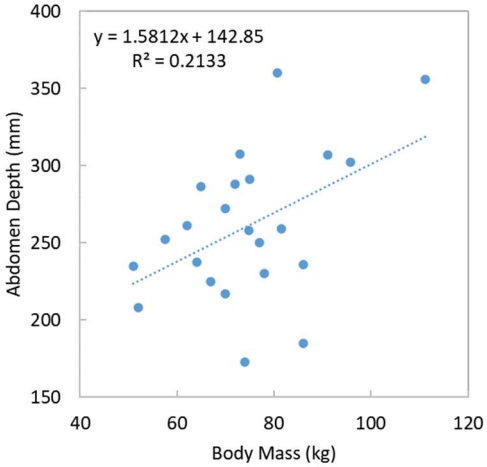

Figure 3. Linear regression fit of abdomen depth and body mass

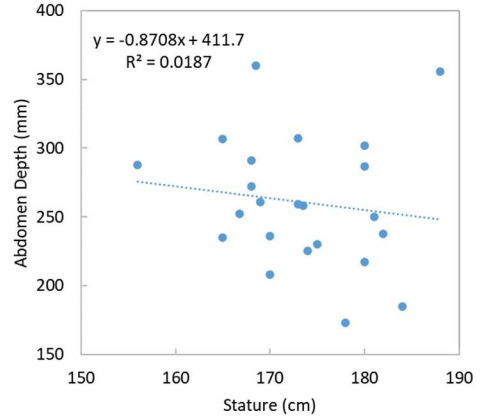

Figure 4. Linear regression fit of abdomen depth and stature

Lumbar Spine Load Case Selection

Selection of the lumbar spine load cases primarily focused on full-body tests. From a human anatomy perspective, the differences between a human lumbar spine and an ATD lumbar spine result in different loading mechanisms in crash test environments. The human lumbar spine has a complex vertebrae joint structure coupled with ligaments and muscles, which are absent in any ATD lumbar spine designs. The load passing through the cross-section of the human lumbar spine (transverse plane) is carried by both the spine and muscles, whereas in ATD designs, the load is mainly carried by the lumbar spine alone. Given these observations, it may not be appropriate to use isolated lumbar spine responses to generate an injury risk function for ATDs in predicting potential injuries in motor vehicle crash (MVC) events. Therefore, full-body PMHS test cases were prioritized for data selection in developing the lumbar injury risk curve.

With these considerations, the following load cases were selected for match-paired tests: Shaw et al. (2009), Crandall (2012), Luet et al. (2012), Uriot et al. (2015), Richardson et al. (2020a), UMTRI test series (32 km/h and 50 km/h), Baudrit et al. (2022), and Guettler et al. (2023). Only male specimens were selected for this analysis. The cases and scaled values for injury risk function fit are summarized in Table 1, and the unscaled and scaled THOR-AV data for the respective PMHS specimens are summarized in Table A1 and A2 in the appendix.

Table 1. List of the load cases for THOR-AV lumbar injury risk function development

PMHS Test References	Load Case Summary	Test/FE
UMTRI	32km/h, 25° seatback, 3.5kN LL, semi-rigid seat	Test
	32km/h, 45°, seatback, 3.5kN LL, semi-rigid seat	Test
	50km/h, 25° seatback, 3.0 kN LL, semi-rigid seat	Test
	50km/h, 45° seatback, 3.0 kN LL, semi-rigid seat	Test
Richardson et al. 2020a	50 km/h, 45°, dual PT, LL, semi-rigid seat	Test
Uriot et al. 2015	50 km/h, 23°, front seat config, semi-rigid seat	Test
	50 km/h, 23°, rear seat config, semi-rigid seat	Test
Luet et al. 2012	config1, 40 km/h, rigid seat, seat pan 0°	FE
	config2, 50 km/h, rigid seat, seat pan 0°	FE
	config3, 50 km/h, rigid seat, sea pan 5°	FE
Shaw et al. 2009	40 km/h, 25° seatback, rigid seat, no LL	FE
Crandall 2012	30 km/h, 25° seatback, rigid seat, 3 kN LL	FE
Baudrit et al. 2022	50 km/h, 60° seatback, semi-rigid, PT, 3.5 kN LL	Test
Guettler et al. 2023	V13, sports utility, rear seat, NCAP85 pulse	Test
	V14, sports utility, rear seat, PT, LL, NCAP85 pulse	Test
	V15, midsize sedan, rear seat, NCAP85 pulse	Test
	V19, midsize sedan, rear seat, PT, LL, NCAP85 pulse	Test

Note: LL – load limiter, PT – pretensioner

Abdomen Load Case Selection

Abdominal injury is typically caused by lap belt loading, especially when occupants submarine. Rouhana et al. (1987 and 1989) demonstrated that the product of force and compression is a good predictor of abdominal injuries using porcine cadavers. They also developed a frangible abdomen for the Hybrid III dummy capable of predicting abdomen injuries during submarining. Miller (1989) found that abdomen injury correlates with the maximum compression and force of belt load in the abdomen of supine, rigidly supported, and anesthetized swine. Hardy et al. (2001) conducted rigid-bar, seatbelt, and close-proximity airbag tests on the abdomen to establish abdominal load-penetration corridors for belt loading at various speeds. Steffan et al. (2002) investigated abdomen response to dynamic lap belt loading at 6 m/s to understand the abdomen injury threshold under belt load. Trosseille et al. (2022) conducted high-speed loading of the abdomen with a seatbelt from 11 m/s to 23 m/s and calculated the stiffness and damping effects on the abdomen. Foster et al. (2006) characterized the response of human cadaver abdomen to high-speed seatbelt loading using pyrotechnic pretensioners and recorded peak penetration and speed

of penetration. Liver injuries were observed in three out of the eight specimens. Lamielle et al. (2008) tested eight male PMHS in an upright seating posture with an instrumented rigid seat. However, these specimens were used for secondary non-injurious pelvis lateral impact and out-of-position tests with frontal airbags before autopsy, making it unclear whether the abdomen injuries were caused by the belt test or subsequent out-of-position airbag test. Howes et al. (2015) conducted six male PMHS tests, four in an inverted position and two in an upright position, achieving a target peak lap belt speed of 3 m/s, resulting in jejunum damage in five of the six tests. Due to lack of belt anchor position and dummy position information, these data were not included in the analysis. Ramachandra et al. (2016) conducted belt tests without back support at a nominal peak penetration speed of 4.0 m/s, observing jejunum tear, colon hemorrhage, omentum tear, splenic fracture, and transverse process fracture during post-test autopsy inspection. Most recently, Guettler et al. (2023) conducted twelve PMHS tests in rear seats to understand submarining behavior using four rear-seat vehicle-bucks, observing abdomen injuries and submarining in these tests. Porcine data from Kent et al. 2006 and 2008, which is close to 6-year-old child response, were used in the past to develop injury risk curves for dummies (Suntay et al. 2021, Beillas et al. 2023). The analysis of Wang et al. 2024 showed large discrepancy between the IRFs created from PMHS and porcine data. Since enough PMHS load cases were identified, the investigation in this study focused on PMHS load cases only.

Table 2. Load case list and peak values of the THOR-AV abdomen pressure output for abdomen injury risk function development

PMHS Test References	Load Cases	Test
Ramachandra et al. 2016	Belt pull, free back, load at T11/T12 level, 4.2 m/s	FE
Foster et al. 2006	A, belt pull, dual PT, fixed back, load at mid umbilicus	FE
	B, belt pull, single PT, fixed back, load at mid umbilicus	FE
	C, belt pull, single PT, fixed back, load at mid umbilicus	FE
Hardy et al. 2001	GI3, free back rigid bar, load at mid-abdomen, 6.3 m/s	FE
	GI6, free back rigid bar, load at mid-abdomen, 6.1 m/s	FE
	GI7, free back rigid bar, load at mid-abdomen, 9.1 m/s	FE
	GI8, free back rigid bar, load at mid-abdomen, 9.0 m/s	FE
	GI10, free back rigid bar, load at upper abdomen, 8.9 m/s	FE
	GI11, free back rigid bar, load at upper abdomen, 6.2 m/s	FE
	CB1/CB3/CB5, seat belt loading, free back,	FE
	CB4/CB6, seat belt loading, free back,	FE
Steffan et al. 2002	test 5, ECE R16 seat, belt load, 6 m/s	FE
	test 6 & 9, ECE R16 seat, lap belt load, 6 m/s	FE
	test 11, ECE R16 seat, lap belt load, 6 m/s	FE
	test 12, ECE R16 seat, lap belt load, 6 m/s	FE
	test 14, ECE R16 seat, lap belt load, 6 m/s	FE
	test 15, ECE R16 seat, lap belt load, 6 m/s	FE
	test 17, ECE R16 seat, lap belt load, 6 m/s	FE
Trosseille et al. 2002	PRT034/035/036, belt pull, fixed back,	FE
Guettler et al. 2023	V13, sports utility, rear seat, NCAP85 pulse	Test
	V14, sports utility, rear seat, PT, LL, NCAP85 pulse	Test
	V15, midsize sedan, rear seat, NCAP85 pulse	Test
	V19, midsize sedan, rear seat, PT, LL, NCAP85 pulse	Test

In summary, Hardy et al. (2001), Steffan et al. (2002), Trosseille et al. (2022), Foster et al. (2006), Ramachandra et al. (2016), and Guettler et al. (2023) were selected as the load cases for developing the abdomen injury risk curve function. Table 2 summarizes the load cases and peak values of the

APTS sensors. The unscaled and scaled THOR-AV data for the respective PMHS specimens are summarized in Table A3 and A4 in appendix 1.

Pelvis Load Case Selection

Pelvic bone fractures are a significant cause of death and residual disability in motor vehicle collisions (MVC). Stein et al. (2006) analyzed data from CIREN centers between 1996 and 2005, finding that among 1,851 patients, 511 (27.6%) had a pelvic fracture, with an overall mortality rate of 17%. Luet et al. (2012) investigated the submarining phenomenon in front crashes with a rigid seat, where the lap belt slides over the anterior superior iliac spine (ASIS). They studied nine PMHS specimens to understand lap belt tensions, pelvic rotation, and lap belt angles. Uriot et al. (2015) modified the rigid seat used by Luet et al., adding springs underneath the seat pan and an anti-submarining plate to simulate the deformation of front and rear sedan production seats. PMHS did not submarine in the frontal seat configuration and experienced no pelvic fractures, but submarining and pelvic fractures were observed in the rear seat configuration. Richardson et al. (2020a) investigated submarining responses using a dual pre-tensioner provided by Autoliv with five PMHS specimens. One specimen submarined, and four suffered pelvic fractures. Baudrit et al. (2022) conducted PMHS tests at a 60° seat back angle, with no submarining observed but pelvic bone fractures observed in all three PMHS specimens. In the University of Michigan Transportation Research Institute (UMTRI) tests at 25° and 45° seat back angles with a moderate speed of 32 km/h, no submarining or pelvic fractures were observed.

Table 3. List of load cases and A.S.I.S. load cell peak values for pelvic injury risk function development

References	Load Case	Test/FE
Luet et al. 2012	config1, 40 km/h, rigid seat, seat pan 0°	FE
	config2, 50 km/h, rigid seat, seat pan 0°	FE
	config3, 50 km/h, rigid seat, sea pan 5°	FE
Uriot et al. 2015	50 km/h, 23°, front seat config, semi-rigid seat	Test
	50 km/h, 23°, rear seat config, semi-rigid seat	Test
Richardson et al. 2020a	50 km/h, 50°, dual PT, 3.5 kN LL,	Test
UMTRI	32 km/h, 25° seatback, 3.5kN LL, semi-rigid seat	Test
	32 km/h, 45° seatback, 3.5kN LL, semi-rigid seat	Test
	50 km/h, 25° seatback, 3.0 kN LL, semi-rigid seat	Test
	50 km/h, 45° seatback, 3.0 kN LL, semi-rigid seat	Test
Baudrit et al. 2022	50 km/h, 60° seatback, semi-rigid, PT, 3.5 kN LL	Test
Guettler et al. 2023	V13, sports utility, rear seat, NCAP85 pulse	Test
	V14, sports utility, rear seat, PT, LL, NCAP85 pulse	Test
	V15, midsize sedan, rear seat, NCAP85 pulse	Test
	V19, midsize sedan, rear seat, PT, LL, NCAP85 pulse	Test

However, in the second UMTRI test series at 50 km/h, pelvic fractures with AIS3 and AIS4 were observed in each test. In production rear seat buck tests conducted by Guettler et al. (2023), submarining and pelvic fractures were observed in some tests.

In summary, sled test conditions that recorded pelvic bone injuries were chosen for injury risk prediction. These tests include Luet et al. (2012), Uriot et al. (2015), Richardson et al. (2020a), UMTRI test series (32 and 50 km/h), Baudrit et al. (2022), and Guettler et al. (2023). The load cases and the peak values are summarized in Table 3, and the unscaled and scaled data are summarized in Table A5 and A6 in appendix 1.

RESULTS

THOR-AV match-paired tests were conducted to develop the injury risk function. In cases where these tests had not yet been performed, the THOR-AV finite element model (v0.7.2) was utilized as a substitute for the physical tests, with plans for future updates.

Lumbar spine injury risk curves

In developing the lumbar injury risk curve, the T12/L1 load cell in the THOR-AV dummy (Humanetics model 10415) measures Fx, Fy, Fz, Mx, and My. In frontal crash accidents, lumbar injuries are primarily caused by forward and downward motions, resulting in bending moments (Mx and My) and compression (Fz) (Packhock et al. 2021, Richardson et al. 2020b).

The moment Mx is relatively small compared to My in the PMHS load cases used in this study. Due to the lack of oblique loading cases, the results may not be accurate for oblique loading conditions. To the authors' knowledge, vertebrae column dislocations caused by pure shear (Fx and Fy) in automotive crashes have not been reported in any literature and were therefore not considered in the analysis.

Figure 5. Moment and compression load to the lumbar spine

To account for the bending moment and compression force of the lumbar spine, Lij was calculated by summing the individual time-histories of Fz normalized by $F_{z_{critical}}$ and Mxy normalized by $M_{xy_{critical}}$ before calculating the peak value (see formula 10).

$$\text{Lij} = \max\left(\frac{F_z(t)}{F_{z_{critical}}} + \frac{M_{xy}(t)}{M_{xy_{critical}}}\right) \qquad (10)$$

Where

$$\text{Mxy(t)} = \sqrt{Mx(t)^2 + My(t)^2} \qquad (11)$$

Peak values of Fz and Mxy were used to fit the survival function. The critical values for Fz and Mxy were determined from the injury risk curve functions for Fz and Mxy. These critical values are defined as twice the injury risk values at a 50% probability of injury, aiming to achieve a value of 1.0 for Lij at its 50% injury risk probability. Log-logistic, lognormal, and Weibull survival functions were fitted with the matched-pair data. The distributions for Maximum Abbreviated Injury Score (MAIS) MAIS2+ and MAIS3+ (AIS 2015) are shown in Figure 6 through Figure 9. The Mxy (for both MAIS2+ and MAIS3+) and Lij (MAIS3+) did not converge in the model fitting, and no plots were generated.

The survival functions for compression force (Fz), Mxy (bending moment), and Lij (combined load index), along with their corresponding injury risk values, are listed in Table 4, 5 and 6. Mxy had a poor

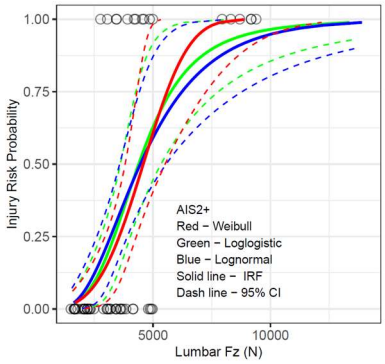

Figure 6. Lumbar compression force Fz MAIS2+ injury risk curve

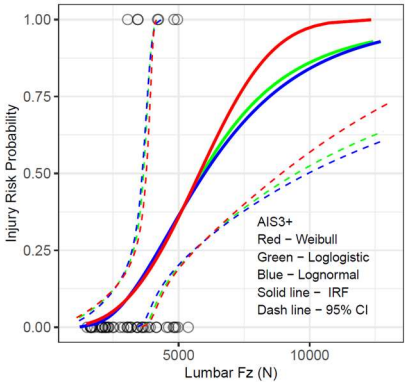

Figure 7. Lumbar spine compression Fz MAIS 3+ injury risk curves

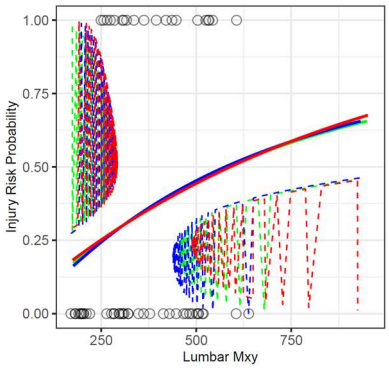

Figure 8. Lumbar spine Mxy MAIS2+ injury risk curves

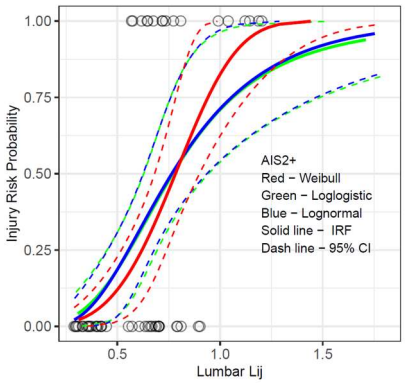

Figure 9. Lumbar spine Lij MAIS2+ injury risk curves

fit for MAIS2+ cases (shown in Figure 7), and did not converge for MAIS3+ cases. No Lij fit was performed for MAIS3+ cases since the Mxy did not converge.

For the quality index, Fz with MAIS2+ are all less than 0.5, indicating good fit. The Fz with MAIS3+ are greater than 0.5, indicating a fit between good and fair. Mxy has quality index values between 1.0 and 1.5, indicating marginal fit. The quality index for Lij is lower than 0.5, indicating a good fit.

As you may have noticed in Table 4 and other tables, different GKG and AUROC values were yielded from different survival fits rather than the same. This is because the GKG and AUROC were calculated after highly influential points were removed using dfbeta. The dfbeta may not remove the same points for different survival fits.

Table 4. Lumbar compression force (Fz) survival functions and injury risk values at 5%, 25% and 50% injury probabilities.

AIS	Fit	Shape	Scale	AIC	GKG	AUROC	Qual. Index	Injury Risk Values (N)		
								5%	25%	50%
MAIS2+	Weibull	3.4798	5095.2745	46.2	0.74	0.836	0.37	2170	3562	4586
	Loglogistic	4.0336	4390.7144	51.4	0.70	0.784	0.39	2116	3344	4391
	Lognormal	2.0129	4460.8910	57.7	0.64	0.784	0.44	1970	3191	4461
MAIS3+	Weibull	1.6509	10046.9899	53.7	0.53	0.77	1.06	1662	4724	8047
	Loglogistic	2.0134	7851.9993	53.4	0.53	0.77	1.19	1819	4550	7852
	Lognormal	1.1951	7846.3245	53.1	0.53	0.77	1.21	1981	4462	7846

Table 5. Lumbar moment Mxy survival functions and injury risk values at 5%, 25% and 50% injury probability.

AIS	Fit	Shape	Scale	AIC	GKG	AUROC	Qual. Index	Injury Risk Values (Nm)		
								5%	25%	50%
MAIS2+	Weibull	1.0167	844.9372	76.9	0.25	0.627	1.40	46	248	589
	Loglogistic	1.3187	581.1463	76.8	0.25	0.627	1.43	62	253	581
	Lognormal	0.8335	575.4939	76.7	0.25	0.627	1.39	80	256	575

Table 6. Lumbar Lij survival functions and injury risk values at 5%, 25% and 50% risk probabilities for MAIS2+ cases.

AIS	Fit	Shape	Scale	AIC	GKG	AUROC	Qual. Index	Injury Risk Values		
								5%	25%	50%
MAIS2+	Weibull	3.76565	0.86306	50.1	0.65	0.83	0.28	0.39	0.62	0.78
	Loglogistic	3.41687	0.77032	61.2	0.56	0.78	0.41	0.33	0.56	0.77
	Lognormal	2.09312	0.76526	60.8	0.56	0.78	0.40	0.35	0.55	0.77

The critical values for Fz and Mxy were selected as twice the injury risk values at 50% injury probability. The critical values for Fz and Mxy for MAIS2+ are 9172 N (4586 N × 2) and 1178 Nm (589 Nm × 2), respectively, for the Weibull fit.

The quantile-quantile (QQ) plots were investigated for Fz, Mxy and Lij Weibull distributions for MAIS2+ and shown in Figure 10, 11 and 12, respectively.

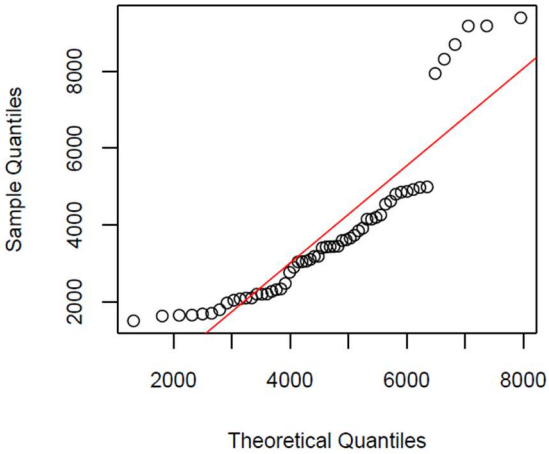

Figure 10. QQ plot of Fz Weibull distribution for MAIS2+

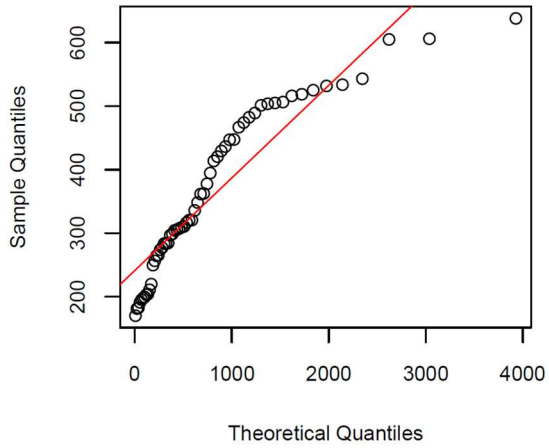

Figure 11. QQ plot of Mxy Weibull distribution for MAIS2+

An investigation was also conducted by removing the data generated from FE analysis, i.e., the load cases from Shaw et al. (2009), Crandall et al. (2012), and Luet et al. (2012), which happened to be cases with no injuries reported. The injury risk curves for compression force Fz are shown in Figure 13 and 14 for MAIS2+ and MAIS3+ only. The moment Mxy and Lij did not converge, and no plots were generated.

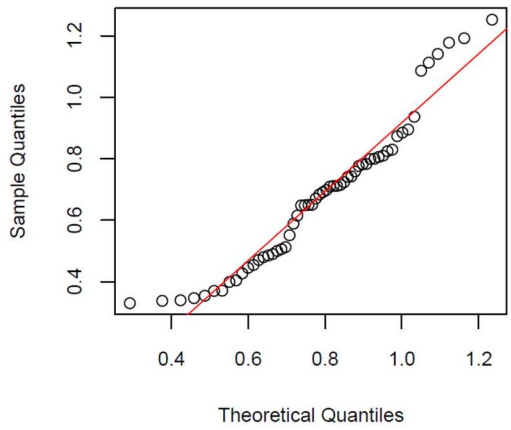

Figure 12. QQ Plot of Lij Weibull distribution for MAIS2+

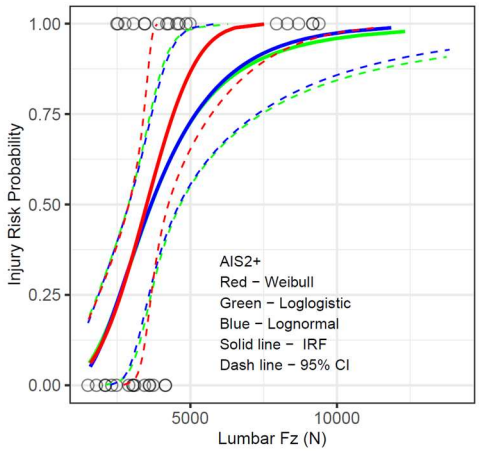

Figure 13. Lumbar compression Fz MAIS2+ injury risk curves with THOR-AV test data only

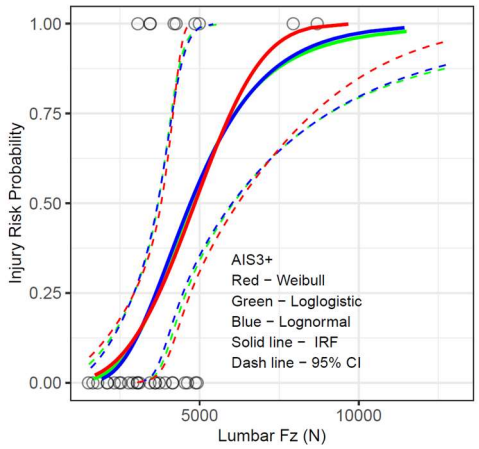

Figure 14. Lumbar compression Fz MAIS3+ injury risk curves with THOR-AV test data only

Abdomen Injury Risk Curves

In the THOR-AV abdomen, APTS pressure sensors were instrumented to measure loading from the lap belt. The maximum pressure recorded by the APTS was used in this analysis. Weibull, log-logistic, and lognormal functions were fitted using matched-pair PMHS data. The distributions for maximum AIS scores, MAIS2+ and MAIS3+, based on PMHS data, are shown in Figure 15 and 16. The scale and shape factors of the abdomen pressure injury risk function, along with the injury risk values at 5%, 25%, and 50% probabilities, are summarized in Table 8.

Table 7. Injury risk values for lumbar compression force Fz with THOR-AV test data only.

AIS	Fit	Shape	Scale	AIC	GKG	AUROC	Quali. Index	Injury Risk Values (N)		
								5%	25%	50%
MAIS2+	Weibull	3.0194	3963.8711	37.3	0.671	0.836	0.38	1482	2624	3511
	Loglogistic	3.1632	3669.6679	43.7	0.567	0.784	0.48	1447	2593	3670
	Lognormal	1.9462	3660.7417	43.4	0.567	0.784	0.47	1572	2589	3661
MAIS3+	Weibull	3.3296	5414.0873	32.9	0.602	0.801	0.49	2219	3724	4850
	Loglogistic	4.3134	4730.0112	33.3	0.642	0.821	0.49	2390	3666	4730
	Lognormal	2.5769	4708.7989	33.0	0.642	0.821	0.49	2487	3624	4709

Table 8. Abdomen pressure injury risk function scale and shape parameters and injury risk values

AIS	Fit	Shape	Scale	AIC	GKG	AUROC	Qual. Index	Injury Risk Values (kPa)		
								5%	25%	50%
MAIS2+	Weibull	3.5054	298.5578	312.8	0.19	0.597	0.23	128	209	269
	Loglogistic	3.9430	275.2554	322.6	0.11	0.557	0.30	130	208	275
	Lognormal	1.7177	260.3630	344.1	0.07	0.536	0.40	100	176	260
MAIS3+	Weibull	3.8799	316.2339	255.6	0.16	0.579	0.23	147	229	288
	Loglogistic	4.4597	293.2402	261.3	0.10	0.550	0.28	152	229	293
	Lognormal	1.7547	290.5577	285.0	0.05	0.524	0.43	114	198	291

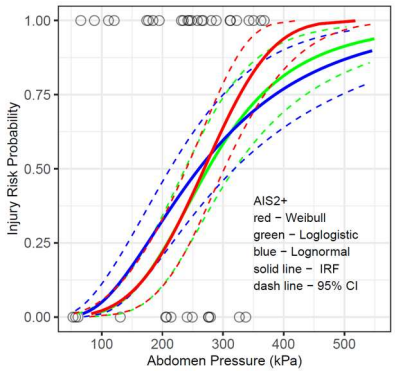

Figure 15. Abdomen MAIS2+ injury risk curves

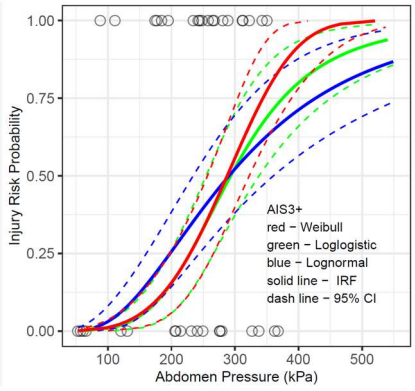

Figure 16. Abdomen MAIS3+ injury risk curves

The QQ plots of abdomen pressure form MAIS2+ and MAIS3+ are shown in Figure 17 and 18 respectively.

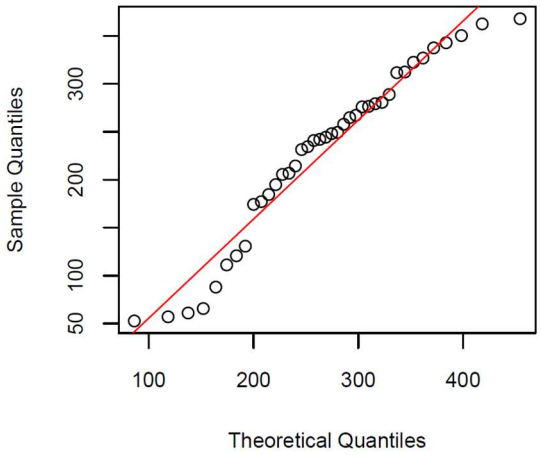

Figure 17. QQ plot of abdomen pressure for MAIS2+

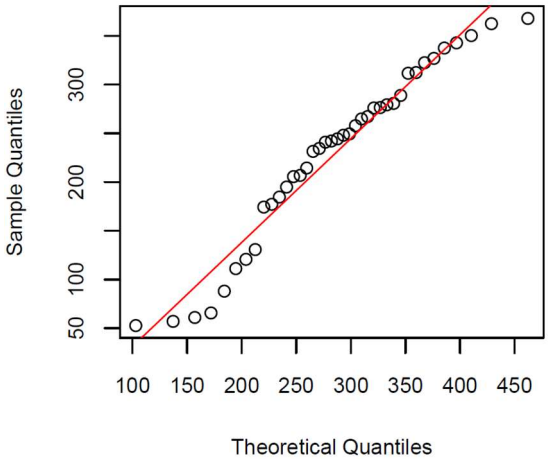

Figure 18. QQ plot of abdomen pressure for MAIS3+

Iliac crest injury risk curves

Iliac crest fractures are typically caused by the lap belt load applied to the anterior superior iliac spine (ASIS) (Garret et al. 1962, Kulowski et al. 1980, Durbin et al. 2001). Another potential cause is acetabulum fracture due to load from the femur, often from the knee bolster (Viano et al. 1988, Parenteau et al. 2003). This study focuses specifically on the lap belt load to the pelvic bone through the ASIS. Two different ASIS force metrics were evaluated: 1) the peak from the time history of the sum of the left and right ASIS X-axis forces, and 2) the peak ASIS X-axis force, which could occur in either the left or right ASIS.

The pelvis MAIS2+ injury risk curves for the total ASIS forces are shown in Figure 19. The maximum of the peak ASIS forces is shown in Figure 20. Please note that the lognormal and loglogistic distributions are nearly overlap each other in Figure 19 and Figure 20. For MAIS3+ analysis, all the injurious case were removed when the data passed through "DFBETA" (detecting influential points in regression) threshold of $\frac{2}{\sqrt{n}}$, where n is the number of samples. No MAIS3+ injury risk function is provided for the iliac crest fracture.

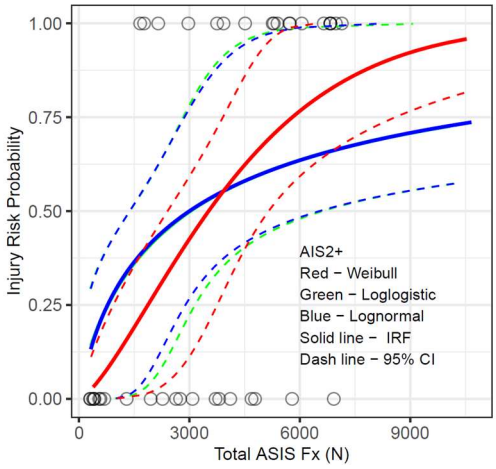

Figure 19. ASIS MAIS2+ fracture injury risk curves for peak of the total ASIS forces

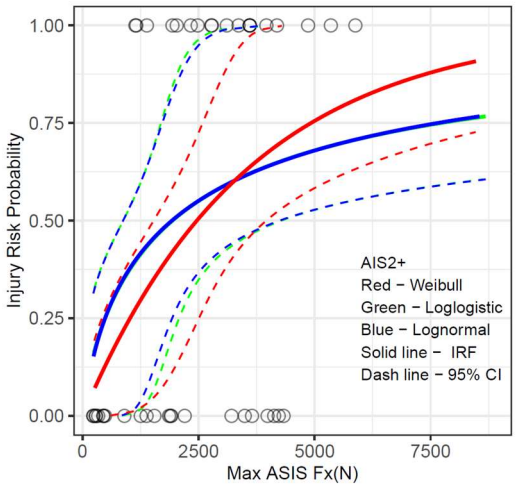

Figure 20. ASIS MAIS2+ fracture injury risk curves for maximum of the left and right peak ASIS forces

The shape and scale factors of the survival functions, along with the injury risk values at the risks of 5%, 25% and 50% probability risks for total ASIS force and maximum ASIS force, are shown in Table 9 and 10, respectively.

Table 9. Injury risk function shape and scale factors and injury risk values for total ASIS force in x-direction.

AIS	Fit	Shape	Scale	AIC	GKG	AUROC	Qual. Index	Injury Risk Values (N)		
								5%	25%	50%
MAIS2+	Weibull	1.3918	4582.4151	44.3	0.63	0.82	0.76	542	1872	3522
	Loglogistic	0.8125	3023.1714	58.6	0.40	0.70	1.56	81	782	3023
	Lognormal	0.4992	2996.6044	58.6	0.40	0.70	1.56	111	776	2997

Table 10. Injury Risk function shape and scale factors and injury risk values for maximum ASIS force in x-direction.

AIS	Fit	Shape	Scale	AIC	GKG	AUROC	Qual. Index	Injury Risk Values (N)		
								5%	25%	50%
MAIS2+	Weibull	1.0008	3551.4901	52.0	0.46	0.73	0.95	183	1023	2462
	Loglogistic	0.7945	1937.1319	59.4	0.36	0.68	1.59	48	486	1937
	Lognormal	0.4891	1925.3407	59.4	0.36	0.68	1.58	67	485	1925

The QQ plot of the total and maximum ASIS forces for MAIS2+ and MAIS3+ are shown in Figure 21, 22, 23 and 24, respectively.

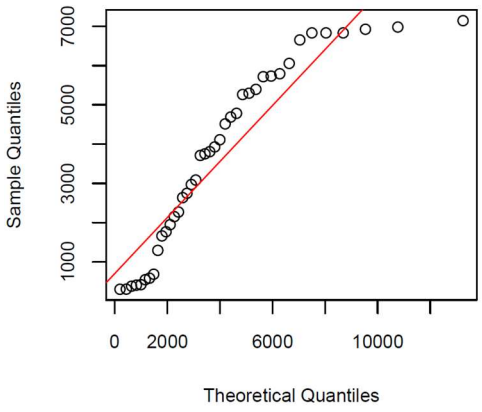

Figure 21. QQ plot of total ASIS force for MAIS2+

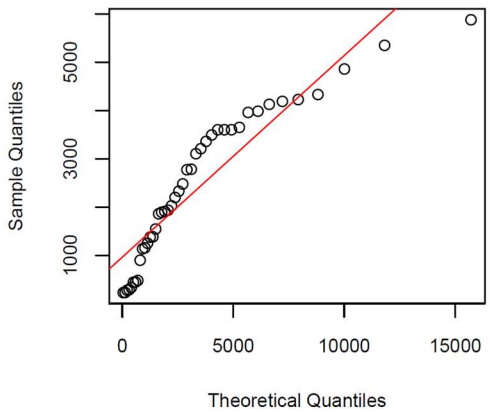

Figure 22. QQ plot of maximum ASIS force for MAIS2+

DISCUSSION

The lumbar spine injury risk function has not been developed for any dummies in the past. With reclined seating, occupants have a higher risk of submarining (Lin et al., 2018; Boyle et al., 2019). The higher compression load in a reclined seat, combined with a forward bending moment, raises concerns about increased lumbar injury risk. An injury risk function would provide quantified information for restraint system development.

A comparison of isolated lumbar spines between Hybrid III and PMHS was conducted under quasi-static and dynamic test conditions by Demetropolos et al. in 1998 and 1999, respectively. The quasi-static tests showed that Hybrid III 50th percentile lumbar responses differ significantly from PMHS lumbar responses: approximately 7 times stiffer in tension, 20 times stiffer in flexion, half as stiff in extension, 5 times stiffer in posterior shear, and 3 times stiffer in lateral shear. In dynamic tests of Hybrid III and PMHS lumbar spines, it was shown that the Hybrid III lumbar spine has much lower stiffness in the initial loading stage, is approximately 2.5 times stiffer in the later loading stage in flexion, and a similar trend was found in extension tests. In THOR and THOR-AV, the lumbar designs are simplified in a concept similar to the Hybrid III, with a uniform cross-section and a steel cable in the center. This design cannot provide distinct responses in flexion, extension, tension, and compression to accurately mimic a human lumbar spine. In this study, the T12 load cell, positioned adjacent to L1, was used for lumbar injury risk assessment. There was interest from a few THOR users in the past to include an L5 load cell to measure lumbar spine loads, as it would capture much higher

load values compared to the L1 position and potentially offer improved injury risk prediction. Jones et al. (2016) investigated lumbar vertebrae fracture injury risk using the Total Human Model for Safety (THUMS), reconstructing four real-world motor vehicle crashes from the Crash Injury Research and Engineering Network (CIREN) and the National Automotive Sampling System - Crashworthiness Data System (NASS-CDS) database. The study clearly distinguished peak compression and bending loads between injury and non-injury cases for loads at L1 through L5. However, the differences in loading magnitudes between injuries and non-injuries at L5 were much smaller compared to L1 through L4. This suggests that the T12/L1 location is adequate for injury prediction measurements, and adding an L5 load cell would not necessarily provide a better indication for lumbar spine injury prediction.

Like the neck Nij development (Mertz et al., 1971, Prasad, et al., 1984, Mertz et al., 2016), the critical values for Fz and Mxy in Lij calculation could be determined and estimated from volunteer tests and adjusted based on in-position test and out-of-position tests. However, the isolated neck has functioning musculature intact for testing while this is impractical for lumbar spine. The lumbar spine is coupled with the torso by the related musculatures and it's difficult to incorporate these muscles as part of the isolated lumbar spine PMHS testing. Therefore, two possible methods were considered to determine the critical values of lumbar compression force and bending moment from the whole body PMHS tests. The first method is to average the matched-pair lumbar loads. The second method is to use the value at 50% injury risk multiplied by two, which would bring the Lij value close to 1.0 for 50% injury risk probability. This is subjective numerical manipulation and does not improve the accuracy of injury prediction. Considering the limited PMHS specimens, the second method would provide a better statistical estimation and was selected in this study.

From Table 4, it shows that Fz Weibull distribution for MAIS2+ is the best indicator to predict injury, with a GKG in 0.74 and an AUROC in 0.863. The Fz has a GKG of 0.568 for MAIS3+, indicating that the relationship is slightly better than a random distribution, which has a GKG of 0.50. It appears that Fz is a strong indicator for AIS2+ injury prediction. From Table 5, it shows that Mxy has a poor fit for MAIS2+ cases, with a GKG of 0.254 and an AUROC of 0.568. It did not converge for MAIS3+ cases. From the results of lumbar spine Lij in Table 6, it shows that the Weibull distribution has the highest GKG and AUROC values at 0.646 and 0.823, respectively. This raises the question of whether Lij for MAIS2+ is a choice suitable for injury prediction, given that it was calculated from Fz and Mxy, and Mxy is a weak injury predictor statistically. A couple of well-known and accepted examples of injury prediction development in the past include the use of accelerations for head injury criterion (HIC) and angular velocities for BrIC calculation for injury predictions. There is no evidence showing that an injury predictor derived from measured input parameters requires each input parameter to be a strong injury predictor. Lij is a new indicator derived from Fz and Mxy and could be evaluated based on its strength for injury prediction statistically.

Given results of AIC, GKG, AUROC, and quality index, Fz is the best injury predictor, followed by Lij for MAIS2+ cases. The injury risk functions for Fz and Lij for MAIS2+ are presented below.

$$P(Fz, MAIS2+) = 1 - e^{-\left(\frac{Fz}{5095.2745}\right)^{3.4798}} \quad (12)$$

$$P(Lij, MAIS2+) = 1 - e^{-\left(\frac{Lij}{0.8642}\right)^{4.3528}} \quad (13)$$

Where

$$\text{Lij} = \frac{F_z}{F_{z_{critical}}} + \frac{M_{xy}}{M_{xy_{critical}}} \quad (14)$$

and

$$\text{Mxy} = \sqrt{Mx^2 + My^2} \quad (15)$$

$$F_{z_{critical}} = 9{,}172\ N,\ M_{xy\_critical} = 1{,}178\ Nm$$

An investigation was carried out for the lumbar injury risk function without FE cases, which are Shaw et al., 2009; Crandall et al., 2012; and Luet et al., 2012. These three cases were non-injury cases. Only Fz with MAIS2+ and MAIS3+ converged, and the results for Weibull distributions are shown in Table 11 for comparison. It is noted that there is a large difference between the results in injury risk values. For example, Fz of MAIS2+ at 25% injury risk has a value of 3562 N with all data, and 2624 N for test data alone. One reason could be that the smaller data set provided different results than the larger data set, considering the load cases are already relatively small for typical statistical analysis. The accuracy of the FE analysis results could play a role, but it should account for a smaller portion compared to the reduced data set due to the validation work, knowing that we could not quantify it until we have both test data and FE results for this exercise.

Table 11 Comparison of Weibull distribution with and without FE data

AIS	Data	Shape	Scale	AIC	GKG	AUROC	Quali. Index	Injury Risk Values (N)		
								5%	25%	50%
MAIS2+	Test + FE	3.4798	5095.2745	46.2	0.74	0.836	0.37	2170	3562	4586
	Test Only	3.0194	3963.8711	37.3	0.671	0.836	0.38	1482	2624	3511
MAIS3+	Test + FE	3.0512	6535.0685	39.3	0.56	0.801	0.86	2469	4344	5795
	Test Only	3.3296	5414.0873	32.9	0.602	0.801	0.49	2219	3724	4850

Table 12 Comparison of lumbar Fz Weibull distribution using either test data or FE data from Richardson et al. 2020 load case.

AIS	Data	Shape	Scale	AIC	GKG	AUROC	Qual. Index	Injury Risk Values (N)		
								5%	25%	50%
MAIS2+	Test	3.47983	5095.27446	46.2	0.74	0.87	0.37	2170	3562	4586
	FE	3.59738	5129.65120	42.1	0.78	0.89	0.35	2247	3628	4633
	Diff.							3.5%	1.9%	1.0%
MAIS3+	Test	1.65095	10046.98990	53.7	0.53	0.77	1.06	1662	4724	8047
	FE	1.79667	9765.41660	52.0	0.56	0.78	0.90	1870	4881	7963
	Diff.							12.5%	3.3%	-1.0%

Since we have both test data and FE results for Richardson et al. 2020 load case. A verification study was carried out to quantify the difference in injury risk function parameters and predicted risk levels when using either the test data or the FE model data as input. The results of lumbar spine Fz risk functions are summarized in Table 12. It is observed the Injury Risk Value differences for 25% and 50% are relatively small, for example 1.9% and 1.0% for MAIS2+, respectively.

Abdomen injury predictions have been extensively explored by many investigators, as reviewed in the introduction section. Albert et al. (2024) investigated abdomen injury risk predictions from belt loading. The evaluated predictors were lap belt force, abdomen compression (Cmax), rate of compression (Vmax), and pressure in the abdominal vasculature. It was found that the best predictors for AIS2+ injuries were pressure and lap belt force, while the best predictor for AIS3+ injuries was V*C. Pressure was a good predictor for both injury risk predictions. Unfortunately, there are no compression measurement sensors in the THOR-AV abdomen design, only twin pressure sensors, and therefore only pressure was assessed in this study. The GKG values are very poor for all the survival fits, and the highest AUROC value from the Weibull fit is 0.579, slightly better than a random distribution. The investigation indicates that pressure from the abdomen pressure sensors is not a strong indicator for abdomen injury prediction. The injury risk functions of the APTS pressure are listed below for reference only.

$$P(p, MAIS2+) = 1 - e^{-\left(\frac{p}{298.5578}\right)^{3.5054}} \quad (15)$$

$$P(p, MAIS3+) = 1 - e^{-\left(\frac{p}{316.2339}\right)^{3.8799}} \quad (16)$$

Beillas et al. (2023) utilized porcine abdomen compression (relative to abdomen depth) and soft compression (relative to compressible abdomen depth only) to develop injury risk curves for a THOR dummy retrofitted with an abdomen designed by the **Ab**domen **I**njury and **Su**bmarining **P**rediction (ABISUP) consortium. No GKG and AUROC values were provided in Beillas et al. (2023) to demonstrate the strength of abdomen pressure as an injury indicator. The log-logistic distribution fit from Beillas et al. (2023) for MAIS3+ showed pressures of 108 kPa, 197 kPa, and 367 kPa for the 25%, 50%, and 75% injury risk curves, respectively. In comparison, the log-logistic fit for MAIS3+ in this study (Table 8) resulted in pressures of 229 kPa, and 288 kPa for 25% and 50% injury risks. These differences likely stem from variations in the designs of the ABISUP abdomen and the THOR-AV abdomen. The ABISUP abdomen was retrofitted to the THOR dummy without any changes to the pelvis. There is a rigid plate behind the abdomen that houses the abdomen pressure sensors (Beillas et al. 2023), which provides immediate support to the abdomen pressure sensors and results in

a quick pressure increase. The THOR-AV design updated the pelvic bone geometry, including the ASIS shape, with the latest geometry (Reed et al. 2013). There is no rigid plate behind the abdomen, but the dummy spine in the THOR-AV design (Wang et al. 2022a); as such, the forces measured by the abdomen pressure sensors are expected to be lower than in the ABISUP abdomen because it takes a much longer travel distance for the pressure sensors to be pushed against the next object, i.e., the lumbar spine.

This study analyzes the risk of pelvic bone fractures caused by the lap belt load. The load on the ASIS was measured using ASIS load cells on both the left and right sides. Pelvic bone fractures can result from complex loading scenarios, and it is uncertain whether the load from one side alone (e.g., the maximum of the left or right side) causes injuries. In this study, the total load and the maximum load from the left and right ASIS load cells of the THOR-AV dummy were investigated for injury risk function development. Once again, the Weibull distribution, which showed the lowest AIC value and the highest GKG and AUROC values, is recommended (Table 9 and 10). The maximum ASIS force showed a low GKG value, indicating a weaker relationship with injuries than the total ASIS force. No injury risk function was provided for MAIS3+ because there were not enough MAIS3+ injury cases, and the data did not converge for survival function fitting. The injury risk function for pelvic bone fractures for MAIS2+ is recommended for ASIS fracture prediction and is presented below.

$$P\left(F_{ASIS_{total}}, MAIS2+\right) = 1 - e^{-\left(\frac{F_{ASIS_{total}}}{4582.4151}\right)^{1.3918}} \quad (17)$$

LIMITATIONS

There are a few limitations in this research. The THOR-AV models may not represent the test data in all cases, though they have been validated under other test conditions. The validation process is an internal procedure at Humanetics for commercial product development. The influence of any discrepancies was not quantified in this study. For the lumbar injury risk function, the critical values were not determined in the traditional way through volunteer tests and adjustments for a specific dummy. Instead, statistical assumptions were made, which could not be validated in this study. Secondly, the GKG and AUROC for the lumbar moment (Mxy) are poor, raising the question of whether Lij is appropriate as a potential injury indicator. For the abdomen injury risk function, all data, except for Guettler et al. (2023), were derived from FE analysis. The time at which the injuries occurred was not reported in most of the literature selected for ATD match-pair tests or simulations, so peak values were used in these cases. It is likely that the injuries occurred before the peak values, which implies the injury risk may have been underestimated. The injury risk functions discussed in this paper were not validated through accident reconstruction tests or correlated with field data. These functions are for reference only, until further correlation is investigated for proper recommendations. The configuration of the physical THOR-AV may have changed throughout the testing due to reinforcement of the pelvis and abdomen skins though the reinforcement most likely would not affect the dummy response from our engineering judgement, however no verifications were carried out to verify the observation.

CONCLUSIONS

THOR-AV, a modified dummy derived from the THOR dummy, was developed to evaluate automobile occupant restraint systems in both upright and reclined postures. In this study, injury risk functions were proposed for the modified body segments of THOR, specifically the lumbar spine, abdomen, and iliac crest of the pelvic bone. Log-logistic, log-normal, and Weibull survival functions were analyzed with 95% confidence intervals. The Akaike Information Criterion (AIC), Goodman-Kruskal Gamma (GKG), and Area Under the Receiver Operating Characteristic Curve (AUROC) were used to assess prediction strength and select the final injury risk functions.

The analysis showed that lumbar Fz is the best indicator for lumbar spine injury, followed by Lij. The Fz injury risk values at 5%, 25%, and 50% probabilities are 2170 N, 3560 N, and 4856 N for MAIS2+, respectively. The Lij injury risk values at 5%, 25%, and 50% probabilities are 0.44, 0.65, and 0.79 for MAIS2+, respectively. The abdomen APTS sensors were not found to be a strong indicator for abdomen injury prediction. The APTS injury risk values at 5%, 25%, and 50% probabilities are 128, 209, and 268 kPa for MAIS2+, respectively. The total ASIS force from the left and right ASIS load cells is a better injury predictor than the maximum ASIS force. The total ASIS force injury risk values at 5%, 25%, and 50% probabilities are 542 N, 1872 N, and 3522 N for MAIS2+, respectively. The injury risk values provided in this study should be used with caution until additional FE model validation is conducted and documented and/or additional physical tests are conducted to supplement FE model data used in the risk function development.

ACKNOWLEDGMENTS

The authors would like to express their sincere gratitude to our partners and collaborators for their invaluable contributions in testing and evaluating the THOR-AV dummy over the past few years. The test data generated through these collaborations were essential for conducting the analysis and developing the injury risk functions presented in this study. Special thanks to Mr. Zaifei Zhou and Mr. Christian Hach of Humanetics Digital Group, who provided the THOR-AV FE model validation data.

REFERENCES

Alber, D., Guettler, A., Kemper, A., Hardy, W., (2024) Evaluation of abdominal injury risk prediction from seatbelt loading, 2024 IRCOBI Conference Proceedings, Sept 11-13, Stockholm, Sweden.

Autonomous Vehicle Occupant Safety Consortium (2023). Investigation of the biofidelity of human body models and ATD models in sled test conditions, The 27th International Technical Conference on the Enhanced Safety of Vehicles (ESV), Yokohama, Japan, April 3-6, 2023 (paper# 000288).

Baudrit, P., Uriot, J., Richard, O., Debray, M., (2022) Investigation of potential injury patterns and occupant kinematics in frontal impact with PMHS in reclined postures. Stapp Car Crash Journal, Vol. 66 (Nov 2022), pp. 1-30.

Beillas, P., Bermond, F., Petit, P., Trosseille, X., Compigne, S., Masuda, M., Baudrit, P., Burleigh, M., Wang. J., Perisse, J., Ramachandra, R., Stammen, J., Richard, O. (2024) Pressure-based abdominal injury prediction for the THOR-50M. 27th International Technical Conference on the Enhanced Safety of Vehicles (ESV), April 3-6, 2023, Yokohama, Japan.

Boyle K., Reed M., Zaseck L., Hu J., (2019). A human modeling study on occupant kinematics in highly reclined seats during frontal crashes, IRCOBI Conference Proceedings, September 11-13, 2019, Florence, Italy.

Craig, M., Parent, D., Lee, E., Rudd, R., Takhounts, E., Hasija V. (2020). Injury criteria for the THOR 50th male ATD. National Highway Traffic Safety Administration, September 2020.

Crandall, J., (2012), ATD Thoracic response test development, gold standard buck condition 2: force limited belt, 30 km/h frontal, NHTSA Biomechanics Database, test # b11468, b11469, b11509, b11510, b11511, NHTSA contract no.: DTNH22-09-H-00247.

Di Domenico, L., Nusholtz, G. (2005). Risk curve boundaries. Traffic Injury Prevention, 6(1), 86–94, https://doi.org/10.1080/15389580590903212.

Demetropoulos C.K., Yang, K.H., Grimm, M.J., Khalil, T.B., and King, A.I. (1998). Mechanical properties of the cadaveric and Hybrid III lumbar spines, 42nd Stapp Car Crash Conference Proceedings, Tempe, Arizona, November 2-4, 1998.

Demetropoulos C.K., Yang, K.H., Grimm, M.J., Artham, K.K., and King, A.I. (1999). High-rate mechanical properties of Hybrid III and cadaveric lumbar spines in flexion and extension. 43rd Stapp Car Crash Conference Proceedings, San Diego, California, October 25-27, 1999.

Durbin, D. R., et al. (2001). Seat-belt syndrome in children: A case report of iliac crest fracture. Pediatric Emergency Care, 17(6), 429-431.

Eppinger, R., Marcus, J., and Morgan, R., "Development of Dummy and Injury index for NHTSA's Thoracic Side Impact Protection Research Program," SAE Technical Paper 840885, 1984, https://doi.org/10.4271/840885.

Garrett, J. W., & Braunstein, P. W. (1962). The seatbelt syndrome: Iliac crest fractures associated with lap belts. Journal of Trauma, 2(3), 220-227.

Gehre, C., Gades, H., Wernicke, P., 2009. Objective rating of signals using test and simulation responses, 21st ESV Conference Proceedings, Stuttgart, Germany, June 13-16, 2009.

Guettler, A.J., Bianco, S.T., Albert, D.L., Boyle, D.M., Kemper, A.R., Hardy, W.N., (2023). Frontal-crash occupant protection in the rear seat: submarining and abdomen/pelvis response in midsized male surrogates, Stapp Car Crash Journal, Vol. (Nov 2023).

Hagedorn, A., Stammen, J., Ramachandra, R., Rhule, H., Thomas, C., Suntay, B., Kang, Y-S, Kwon H.J., Moorhouse, K., and Bolte IV, J.H., (2022) Biofidelity evaluation of THOR-50M in rear-facing seating configurations using an update biofidelity ranking system. SAE International Journal of Transportation Safety, Vol. 10, No. 2 (2022), pp. 291-376. https://www.jstor.org/stable/27215865.

Howes, M.K., Hardy, W.N., Agnew, A., Hallman, J.J., (2015). Evaluation of the kinematic responses and

potential injury mechanisms of the jejunum during seatbelt loading. Stapp Car Crash Journal, Vol. 59 (Nov 2015), pp. 225-267.

Humanetics THOR-AV 50M dummy FE model technical report and user's manual, LS-DYNA release version 0.7.2, March 2024. Humanetics Innovation Solutions, Inc., Tel: +1 248 778 2000, fe.support@humaneticsgroup.com.

International Organization for Standardization (ISO). (2014). Procedure to construct an injury

risk curves for the evaluation of road user protection in crash tests. (ISO TS18506)

Lin H., Gepner B, Wu T., Forman J., Panzer M., (2018). Effect of seatback recline on occupant model response in frontal crashes. IRCOBI Conference Proceedings, September 12-14, 2018, Athens, Greece,

Jones D.A., Gaewsky, J.P., Kelley M.R. Weaver, A.A., Miller A.N., Stitzel J.D., (2016) Lumbar vertebrae fracture injury risk in finite element reconstruction of CIREN and NASS frontal motor vehicle crashes, Traffic Injury Prevention, Vol.17: sup1, 109-115, DOI: 10.1080/15389588.2016.1195495

Jorlöv, J. Bohman, K., Larsson, A. (2017). Seating positions and activities in highly automated cars – a qualitative study of future automated driving scenarios, IRCOBI Conference Proceedings, September 13-15, 2017, Antwerp, Belgium.

Kent, R.W., Funk, J.R. (2004) Data censoring and parametric distribution assignment in the development of injury risk functions from biomechanical data. SAE Paper # 2004-01-0317, Society of Automotive Engineers, Warrendale, PA.

Kent, R., Stacey S., Kindig M., Forman J., Woods, W., Rouhana S.W., Higuchi K., Tanji, H., St. Lawrence S., Arbogast K.B. (2006). Biomechanical response of the pediatric abdomen, part I: development of an experimental model and quantification of structural response to dynamic belt loading, Stapp Car Crash Journal, Vol. 50, pp. 1-26.

Kent, R., Stacey S., Kindig M., Woods, W., Evans J., Rouhana, S.W., Higuchi, K., Tanji, H., St. Lawrence, S., Arbogast K.B. (2008) Biomechanical response of the pediatric abdomen, part 2: injuries and their correlation with engineering parameters. Stapp Car Crash Journal, Vol 52, pp. 135-166.

Kitagawa, Y., Hayashi, S., Yamada, K., Gotoh M. (2017). Occupant kinematics in simulated autonomous driving vehicle collisions: influence of seating position, direction, and angle. Stapp Car Crash Journal, Vol. 61 (Nov 2017), pp. 101-155.

Kulowski, J., & Chandler, H. P. (1980). Biomechanical analysis of pelvic fractures due to lap belt restraint in automotive accidents. Automotive Safety Research Journal, 5(1), 45-52.

Kuppa, S., Eppinger, R., McKoy, F., Nguyen, T. (2003) Development of side impact thoracic injury criteria and their application to the modified ES-2 dummy with rib extensions (ES-2re). Stapp Car Crash Journal, Vol. 47: 189-210.

Lamielle, S., Vezin, P., Verriest, J-P., Petit, P., Trosseille, X. Vallancien, G., (2008). 3D deformation and dynamics of the human cadaver abdomen under seatbelt loading. Stapp Car Crash Journal, Vol. 52 (Nov 2008), pp. 267-294.

Mertz, H., "A Procedure for Normalizing Impact Response Data," SAE Technical Paper 840884, 1984, https://doi.org/10.4271/840884.

Mertz, H., and Patrick, L., (1971) Strength and Response of the Human Neck , SAE Technical Paper 710855, 1971, https://doi.org/10.4271/710855.

Mertz, H. J., Prasad, P. and Nusholtz, G. (1996) Head injury risk assessment for forehead impacts. SAE Paper #960099, https://doi.org/10.4271/960099.

Mertz HJ, Irwin AL, Prasad P. Biomechanical and Scaling Basis for Frontal and Side Impact

Injury Assessment Reference Values. Stapp Car Crash J. 2016 Nov;60:625-657. doi:10.4271/2016-22-0018. PMID: 27871108.

Miller, M.A., (1989). The biomechanical response of the lower abdomen to belt restraint loading. The Journal of Trauma: Injury, Infection, and Critical Care 29(11): p1571-1584, November 1989. DOI: 10.1097/00005373-198911000-00019.

NASA Technology, NASA standards inform comfortable car seats, NASA Transportation Spinoff 2013, pg. 60-61, https://ntrs.nasa.gov/api/citations/20140000084/downloads/20140000084.pdf

Mishra, E., & Lubbe, N. (2024). Assessing injury risks of reclined occupants in a frontal crash preceded by

braking with varied seatbelt designs using the SAFER Human Body Model. Traffic Injury Prevention, 25(3), 445–453. https://doi.org/10.1080/15389588.2024.2318414.

Moorhouse, K. (2013). An improved normalization methodology for developing mean human response curves, 23rd International Technical Conference on the Enhanced Safety of Safety of Vehicles (ESV), Seoul, Korea, May 27-30, 2013.

Nusholtz, G., Mosier, R. (1999) Consistent Threshold Estimate for Doubly Censored Biomechanical Data. SAE Paper #1999-01-0714, https://doi.org/10.4271/1999-01-0714.

Ostermaier, I., Sandner, V., Kolke, R., Future seat positions, investigating the impact of novel seat position on occupant safety in connection with automated driving, as demonstrated by sled tests and a vehicle crash test, 2020 Report, ADAC Technik Zentrum, Landsberg am Lech, Germany.

Pachocki, L., Daszkiewicz, K., Luczkiewicz, P., Witkowski, W., (2021) Biomechanics of lumbar spine injury in road barrier collision – finite element study. Front. Bioeng. Biotechnol. 31 Oct 2021, Sec. Biomechanics Volume 9 – 2021, https://doi.org/10.3389/fbioe.2021.760498

Parenteau, C. S., et al. (2003). "Injury patterns of the pelvis and lower extremities in frontal collisions." SAE Technical Paper, 2003-01-0160.

Prasad, P. (2019). ATD seating in highly reclined seats, SAE Government Industry Meeting, April 3-5, 2019. Washington, DC. https://www.nhtsa.gov/sites/nhtsa.gov/files/documents/atd_seating_in_highly_reclined_seats.pdf.

Ramachandra, R., Kang, Y-S., Bolte IV, J.H., Hagedorn, A., Herriott, R., Stammen, J.A. and Moorhouse, K., (2016). Biomechanical responses of PMHS subjected to abdominal seatbelt loading, Stapp Car Crash Journal, Vol. 60 (Nov 2016), pp. 59-87.

Rhule, H., Sticklin, J., Donnelly, B., Moorhouse, K., 2018. Improvements to NHTSA's Biofidelity Ranking System and Application to the Evaluation of the THOR 5th Female Dummy, 2018 IRCOBI Conference Proceedings, September 12 -14, 2018, Athens, Greece.

Richardson, R., Donlon J-P., Jayathirtha, M., Forman, J.L., Shaw, G., Gepner, B., Kerrigan, J.R., Östling, M., Mroz, K., Pipkorn, B. (2020a) Kinematic and injury response of reclined PMHS in frontal impacts. Stapp Car Crash Journal, Vol. (Nov 2020), pp. 83-153.

Richardson, R., Jayathirtha, M., Chastain, K., Donlon J-P, Forman, J., Gepner, B., Ostling M., Mroz, K., Shaw, G., Pipkorn, B., Kerrigan, J., (2020b) Thoracolumbar spine kinematics and injuries in frontal impacts with reclined occupants, Traffic Injury Prevention, 21:sup1, S66-S71, DOI: 10.1080/15389588.2020.1837365

Reed, M.P. (2013). Development of anthropometry specifications for Warrior Injury Assessment Manikin (WIAMan), Final Report, UMTRI-2013-38.

Reed, M.P., Ebert, S.M., Jones L.H. (2019). Posture and belt fit in reclined passenger seats, Traffic Injury Preventions 2019, Vol.20, No. S1, S38-S42, https://doi.org/10.1080/15389588.2019.1630733

Petitjean, A., Trosseille, X., Petit, P., Irwin, A., Hassan, J., Praxl, N. (2009). Injury risk curves for the WorldSID 50th male dummy. Stapp Car Crash Journal, Vol. 53 (Nov. 2009), pp. 443-476.

Petitjean, A., Trosseille, X. (2011). Statistical simulations to evaluate the methods of the construction of injury risk curves. Stapp Car Crash Journal, 2011, Vol. 55. Pp. 411-440. doi: 10.4271/2011-22-0015.

Rouhana, S.W., (1987). Abdominal injury prediction in lateral impact – an analysis of the biofidelity of the Euro-SID abdomen. Proceedings of the 31st Stapp Car Crash Conference, pp. 95-104, New Orleans, Louisiana.

Rouhana, S.W., Viano, D.C., Jedrzejczak, E.A. and McCleary, J.D., (1989), Assessing submarining and abdominal injury risk in the Hybrid III family of dummies, Proceedings of the 33rd Stapp Car Crash Conference, Washington D.C., October 4-6, 1989.

Prasad, P., and Daniel, R., (1984). A Biomechanical Analysis of Head, Neck, and Torso Injuries to Child Surrogates Due to Sudden Torso Acceleration, SAE Technical Paper 841656, 1984, https://doi.org/10.4271/841656.

Stein, D.M., O'Connor, J.V., Kufer, J.A., Dischinger, P.C., Copeland, C.E., Scalea, T.M., (2006), Risk factors associated with pelvis fractures sustained in motor vehicle collisions involving newer vehicles. J Trauma. 2006 Jul;61(1):21-30; discussion 30-1. doi: 10.1097/01.ta.0000222646.46868.cb.

Suntay, B., Stammen, J., Carlson, M., Ramachandra, R. (2021) Abdominal and thoracic injury risk functions for the large omni-directional child (LOCD) ATD. 2021 IRCOBI Conference Proceedings. Sept 8-10, online.

Tarrière, C., (1995) Children are not miniature adults, 1995 IRCOBI Conference Proceedings, Sept 13-15, 1995. Brunnen, Switzerland.

Wang, Z.J., Lober, B., Tesny, A., Hu, G., Kang, Y-S. (2021). Neck biofidelity comparison of THOR-AV, THOR and Hybrid III 50th dummies. IRCOBI Conference Proceedings, Sept 8-10, 2021, online.

Wang, Z.J., Richard, O., Lebarbé, M., Uroit, J., Kabadayi, E., Kleessen, C. (2022a) Biomechanical responses of THOR-AV in a semi-rigid seat that mimics the front and rear seat of a midsize car. IRCOBI Conference Proceedings, Sept 14-16, 2022, Porto, Portugal.

Wang, Z.J., Zaseck, L.W., Reed, M.P. (2022b). THOR-AV 50th percentile male biofidelity in 25° and 45° seatback angle test conditions with a semi-rigid seat. IRCOBI Conference Proceedings, Sept 14-16, 2022, Porto, Portugal.

Wang, Z. (2022c). Biomechanical responses of the THOR-AV ATD in rear racing test conditions. SAE Int. J. Adv. & Curr. Prac. in Mobility 4(6):2089-2105, 2022, https://doi.org/10.4271/2022-01-0836.

Wang, Z.J., Hu, G. (2024) Investigation of pressure-based abdomen injury risk function with postmortem human subject and porcine data for THOR-AV 50M dummy. 2024 IRCOBI Conference Proceedings, Sept. 11-13, Stockholm, Sweden.

University of Michigan Transportation Research Institute (UMTRI), Automated Vehicle Occupant Kinematics, NHTSA Biomechanics Database. The first test series (32 km/h): test numbers b12795, b12796, b13109, b13110, b13119, b13124. PMHS corridors were created by Wang et al. (2022b). The second test series (50 km/h): test numbers b13193, b13194, b13195, b13196.

Viano, D. C., & Lau, I. V. (1988). "Pelvic injuries in frontal impacts: Influence of occupant restraint and direction of load." Journal of Biomechanics, 21(3), 191-205.

Viano, D., Biomechanical responses and injuries in blunt lateral impact," 33rd Stapp Car Crash Conference Proceedings. SAE Technical Paper 892432, 1989, https://doi.org/10.4271/892432.

APPENDIX 1

THOR-AV was designed to represent a 50th percentile male, which has 76 kg total mass and 175 cm stature. The scaling in this paper used the 76 kg weight and 175 cm stature for all scaling calculations. Test and FE results for Richardson et al. 2020a data are both available, however, only the test data were used in the analysis.

Table A1 Maximum values of THOR-AV T12 load cell output (unscaled).

Load Cases	Fz(N)	Fxy (N)	My(Nm)	Mxy (Nm)	Test or FE
UMTRI, 32 km/h, 25°	-2286	877	197.7	198.3	Test
UMTRI, 32km/h, 45°	-3043	1270	216.5	219.9	Test
UMTRI, 50km/h, 25°	-4202	1217	305.6	307.1	Test
UMTRI-52kph-45deg	-8907	1362	354.8	357.5	Test
Richardson et al. 2020a	-4919	644	287.4	288.3	Test
Richardson et al. 2020a	-4892	625	351	355	FE (not used in IRF)
Uriot et al. 2015, frontal	-4588	2318	517.9	539.5	FE
Uriot et al. 2015, rear	-2748	2833	600.7	602.1	FE
Luet et al. 2006, Config1	-3915	1599	405.6	405.6	FE
Luet et al. 2006, Config2	-3830	1868	487.9	494.2	FE
Luet et al, 2006, Config3	-5770	2286	578.0	582.2	FE
Shaw et al. 2009	-2145	1553	284.8	288.0	FE
Crandall et al. 2012	-1735	571	202.6	205.6	FE
Baudrit et al. 2022	-9342	3180.1	288.3	288.7	FE
Guettler et al. 2023, V13	-3328	4096.4	417.4	422.6	Test
Guettler et al. 2023, V14	-1600	1988.4	478.5	502.0	Test
Guettler et al. 2023, V15	-3450	3876.2	475.2	479.2	Test
Guettler et al. 2023, V19	-3802	1601.9	566.9	574.7	Test

Table A2. THOR-AV T12 load cell outputs scaled to the respective PMHS specimen

References	Test #	Specimen #	Sex	Age (yr)	Mass (kg)	Stature (cm)	AIS	λm	λk	λL	Fx (N)	Fy(N)	Fz(N)	Fxy (N)	Mx (Nm)	My (Nm	Mxy (Nm
Shaw et al. 2009	1294	411	M	76	70	178	0	0.921	1.017	1.017	1121	1015	-2077	1503	51	280	284
	1295	403	M	47	68	177	0	0.895	1.011	1.011	1101	997	-2041	1477	49	274	277
	1358	425	M	54	79	177	0	1.039	1.011	1.011	1187	1075	-2200	1592	53	295	299

References	Test #	Specimen #	Sex	Age (yr)	Mass (kg)	Stature (cm)	AIS	λm	λk	λL	Fx (N)	Fy(N)	Fz(N)	Fxy (N)	Mx (Nm)	My (Nm	Mxy (Nm
	1359	426	M	49	76	184	0	1.000	1.051	1.051	1187	1075	-2200	1592	55	307	311
	1360	428	M	57	64	175	0	0.842	1.000	1.000	1062	962	-1969	1425	47	261	264
	1378	443	M	72	81	184	0	1.066	1.051	1.051	1225	1110	-2271	1644	57	317	321
	1379	433	M	40	88	179	0	1.158	1.023	1.023	1260	1141	-2335	1690	57	317	321
	1380	441	M	37	78	180	0	1.026	1.029	1.029	1189	1077	-2204	1595	54	301	304
Crandall et al. 2012	S0028	494	M	59	68	178	0	0.895	1.017	1.017	496	432	-1655	544	37	197	199
	S0029	492	M	66	70	179	0	0.921	1.023	1.023	504	439	-1684	554	38	201	204
	UVAS00302	674	M	67	68	177	0	0.895	1.011	1.011	494	431	-1650	543	36	195	198
	UVAS00303	736	M	67	68	173	0	0.895	0.989	0.989	489	426	-1631	537	35	188	191
	UVAS00304	695	M	74	70	183	0	0.921	1.046	1.046	510	444	-1702	560	39	208	211
Luet et al. 2012	Config 1	631	M	67	59.5	171.5	0	0.783	0.980	0.980	1387	619	-3429	1400	57	348	348
	Config 1	632	M	85	69.5	167	0	0.914	0.954	0.954	1480	660	-3658	1493	59	362	362
	Config 1	633	M	76	54	163	0	0.711	0.931	0.931	1289	575	-3185	1301	50	307	307
	Config 2	634	M	68	79	170	0	1.039	0.971	0.971	1814	887	-3849	1877	124	476	482
	Config 2	635	F	56	57	161	0	0.750	0.920	0.920	1500	733	-3182	1552	97	373	378
	Config 2	636	M	77	61.5	171	0	0.809	0.977	0.977	1606	785	-3406	1661	111	424	429
	Config 3	637	M	79	57	161.5	0	0.750	0.923	0.923	1854	1036	-4800	1902	95	444	447
	Config 3	638	M	67	58	170.5	0	0.763	0.974	0.974	1922	1074	-4975	1971	104	486	489
	Config 3	639	M	90	71	162	0	0.934	0.926	0.926	2073	1158	-5366	2126	106	498	501
Uriot et al. 2015(rear)	SubBIO_22	683	M	55	92	177	0	1.211	1.011	1.011	3108	589	-3041	3135	80	672	674
	SubBIO_23	679	M	86	67	168	2	0.882	0.960	0.960	2584	490	-2528	2607	63	531	532
	SubBIO_24	681	M	87	77	175	2	1.013	1.000	1.000	2828	536	-2766	2852	72	605	606
	SubBIO_25	682	M	87	64	171	3	0.842	0.977	0.977	2548	483	-2493	2570	63	532	534
Uriot et al. 2015 (front)	SubBIO_26	678	M	85	79	165	2	1.039	0.943	0.943	1428	2138	-4542	2295	163	483	504
	SubBIO_27	677	M	84	57	170	2	0.750	0.971	0.971	1231	1843	-3916	1979	145	429	447
	SubBIO_28	676	M	84	64	170	0	0.842	0.971	0.971	1304	1953	-4150	2097	153	455	474
	SubBIO_29	680	M	89	77	175	2	1.013	1.000	1.000	1452	2174	-4618	2334	176	521	543
Richardson et al. 2020a	529	930	M	66	74	175	3	0.974	1.000	1.000	422	-557	-4854	635	60	284	284
	530	630	M	53	57	175	3	0.750	1.000	1.000	370	-489	-4260	558	53	249	250
	531	901	M	72	74	185	3	0.974	1.057	1.057	434	-573	-4990	653	65	308	309

References	Test #	Specimen #	Sex	Age (yr)	Mass (kg)	Stature (cm)	AIS	λm	λk	λL	Fx (N)	Fy(N)	Fz(N)	Fxy (N)	Mx (Nm)	My (Nm	Mxy (Nm
	532	662	M	25	75	174	0	0.987	0.994	0.994	424	-560	-4872	638	60	283	284
	533	815	M	55	74	180	0	0.974	1.029	1.029	428	-565	-4922	644	62	296	297
UMTRI 32 km/h, 25°	b12796/AV20	F2012	M	72	64.4	174.2	0	0.847	0.995	0.995	639	-558	-2100	805	-25	181	181
	b13109/AV21	WSU7	M	80	80.28	170.1	0	1.056	0.972	0.972	705	-615	-2317	888	-27	195	195
	b13124/AV21	S2107	M	70	63.72	175.6	0	0.838	1.004	1.004	639	-557	-2097	804	-25	182	183
UMTRI 32 km/h, 45°	b12795/AV20	35764	M	91	76.1	174.9	0	1.001	0.999	0.999	1147	-598	-3044	1271	-45	216	220
	b13110/AV21	WSU7	M	85	71.1	169.7	0	0.936	0.970	0.970	1092	-569	-2899	1210	-42	200	203
	b13119/AV21	WSU7	M	71	53	166.3	0	0.697	0.950	0.950	933	-486	-2477	1034	-35	167	170
UMTRI 50	b13196/AV22	WSU0	M	71	76.1	174.3	3	1.001	0.996	0.996	-959	-1173	-4197	1216	79	304	305
UMTRI 50 km/h, 45°	b13193/AV22	C2200	M	62	60.8	173.9	3	0.800	0.994	0.994	1079	-649	-7941	1214	-57	314	317
	b13194/AV22	I22040	M	58	65.8	176.1	2	0.866	1.006	1.006	1129	-679	-8313	1271	-61	333	336
	b13195/AV22	WSU0	M	63	82	172.2	2	1.079	0.984	0.984	1247	-750	-9177	1403	-66	360	362
Baudrit et al. 2022	1	746	M	73	69	167	3	0.908	0.954	0.954	2958	605	-8695	2960	88	256	256
	2	744	M	88	76	169	2	1.000	0.966	0.966	3123	639	-9180	3125	94	274	274
	3	745	M	90	84	160	3	1.105	0.914	0.914	3194	654	-9391	3197	91	265	265
Guettler et al. 2023	V13-4	SM129	M	79	63	178	3	0.829	1.017	1.017	3761	1096	-3056	3761	-116	390	395
	V13-5	SM155	M	65	85	168	3	1.118	0.960	0.960	4244	1237	-3448	4245	-123	415	420
	V13-6	SM161	M	83	81	175	4	1.066	1.000	1.000	4229	1233	-3435	4229	-128	431	436
	V14-5	SN156	M	68	89	188	0	1.171	1.074	1.074	2114	-1086	-1795	2230	-185	577	605
	V14-6	SM157	M	59	68	173	0	0.895	0.989	0.989	1773	-910	-1505	1870	-143	445	467
	V14-7	SM160	M	74	79	178	2	1.039	1.017	1.017	1938	-995	-1645	2045	-161	500	525
	V15-5	SM152	M	63	81	180	0	1.066	1.029	1.029	4046	-272	-3612	4058	-55	512	516
	V15-6	SM153	M	51	64	168	0	0.842	0.960	0.960	3475	-233	-3102	3485	-44	410	414
	V15-7	SM165	M	51	89	175	0	1.171	1.000	1.000	4182	-281	-3733	4195	-56	514	519
	V19-5	SM154	M	74	89	178	0	1.171	1.017	1.017	-932	-1722	-4149	1748	-118	629	638
	V19-6	SM095	M	74	64	170	0	0.842	0.971	0.971	-772	-1427	-3438	1449	-94	498	505
	V19-7	SM159	M	29	73	163	0	0.961	0.931	0.931	-808	-1493	-3596	1515	-94	499	506

Table A3. THOR-AV Abdomen Pressures Measurements from the load cases (unscaled)

	Max APTS Left	Max APTS Right	Test or FE
Ramachandra 2016	1.7776	1.8149	FE
Foster et al. 2006 (A)	1.0749	0.8781	FE
Foster et al. 2006 (B)	2.4615	2.5000	FE
Hardy et al. 2001 GI3	1.9301	1.9415	FE
Hardy et al. 2001 GI6	1.9073	1.9132	FE
Hardy et al. 2001 GI7	2.2130	2.2166	FE
Hardy et al. 2001 GI8	2.1861	2.1866	FE
Hardy et al. 2001 GI10	0.1552	0.1560	FE
Hardy et al. 2001 GI11	0.1067	0.1064	FE
Hardy et al. 2001 CB1/CB3/CB5	0.6857	0.6764	FE
Hardy et al. 2001 CB4/CB6	0.7418	0.7610	FE
Steffan et al. 2002 test 5	2.6365	2.4449	FE
Steffan et al. 2002 test 6 & 9	2.3975	2.3144	FE
Steffan et al. 2002 test 11	2.8561	2.6776	FE
Steffan et al. 2002 test 12	2.8695	2.6914	FE
Steffan et al. 2002 test 14	2.9850	2.7860	FE
Steffan et al. 2002 test 15	2.8119	2.7114	FE
Steffan et al. 2002 test 17	2.9534	2.7995	FE
Trosseille et al. 2002	0.5978	0.5074	FE
Guettler et al. 2023 (V13)	0.1266*	2.5935	Test
Guettler et al. 2023 (V14)	0.1204*	2.9084	Test
Guettler et al. 2023 (V15)	0.1493*	3.2699	Test
Guettler et al. 2023 (V19)	0.1612*	3.8461	Test

*The left abdomen pressure sensor malfunctioned, which is very low. These data were excluded from the analysis.

Table A4. THOR-AV abdomen pressure scaled to the respective PMHS specimen

References	Test ID	Specimen No.	Sex	Age	Mass (kg)	Stature (cm)	BMI	AIS	Abdomen Depth (mm)	Abdomen Circum. (mm)	λm	λk	λL	λp	APTS (Bar)
Hardy et al. 2001	GI3	28682	M	87	73	173	24.4	4	307		0.961	0.878	0.989	0.898	1.742864
	GI6	28838	M	85	91	165	33.4	3	307		1.197	0.880	0.943	0.912	1.771418
	GI7	28879	M	74	77	181	23.5	3	250		1.013	1.080	1.034	1.119	2.480407
	GI8	28889	M	71	64	182	19.3	4	238		0.842	1.136	1.040	1.058	2.344791
	GI10	29084	M	64	65	180	20.1	5	287		0.855	0.942	1.029	0.950	0.148081
	GI11	29115	M	74	75	168	26.6	5	291		0.987	0.928	0.960	0.882	0.094096
	CB3	29116	M	78	52	170	18.0	0	208		0.684	1.298	0.971	0.889	0.609791
	CB5	29131	M	88	72	156	29.6	0	288		0.947	0.938	0.891	0.749	0.569885
Steffan et al. 2002	5	-	M	47	75	190	20.8	0		795	0.987	1.195	1.086	1.280	3.374936
	6	-	M	49	85	182	25.7	0		935	1.118	1.016	1.040	1.153	2.764314
	9	-	M	58	100	174	33.0	0		1210	1.316	0.785	0.994	1.005	2.409055
	11	-	M	59	95.5	180	29.5	0		1020	1.257	0.931	1.029	1.145	3.268848
	12	-	M	50	75	175	24.5	0		990	0.987	0.960	1.000	0.973	2.792359
	14	-	M	66	52	169	18.2	3		780	0.684	1.218	0.966	0.851	2.442924
	15	-	M	54	79.3	172	26.8	0		960	1.043	0.990	0.983	0.982	2.76018
	17	-	M	69	72.2	183	21.6	3		965	0.950	0.984	1.046	1.058	3.123292
Trosseille et al. 2002		MS503	M	76	78	175	25.5	2	230		1.026	1.174	1.000	1.098	0.65622
		MS505	M	81	70	168	24.8	1	272		0.921	0.993	0.960	0.881	0.526834
		MS507	M	85	51	165	18.7	5	235		0.671	1.149	0.943	0.781	0.466669
Foster et al. 2006	A-1	31658	M	24	95.7	180	29.5	2	302		1.259	0.894	1.029	1.123	1.206609
	A-2	31996	M	58	111.2	188	31.5	0	356		1.463	0.758	1.074	1.216	1.306809
	A-3	750	M	80	57.6	166.8	20.7	3	252		0.758	1.071	0.953	0.819	0.879979
	A-4	32016	M	83	81.6	173	27.3	3	259		1.074	1.042	0.989	1.034	1.111364
	B-1	31719	M	85	80.7	168.5	28.4	0	360		1.062	0.750	0.963	0.827	2.068326
	B-2	623	M	45	74.8	173.5	24.8	0	258		0.984	1.047	0.991	0.998	2.493869
	B-3	694	M	59	62.1	169	21.7	0	261		0.817	1.034	0.966	0.857	2.143545
	01	PMHS01	M	59	86	170	29.8	3	236		1.132	1.144	0.971	1.074	1.948643
	03	PMHS03	M	66	70	180	21.6	0	217		0.921	1.244	1.029	1.133	2.055443

References	Test ID	Specimen No.	Sex	Age	Mass (kg)	Stature (cm)	BMI	AIS	Abdomen Depth (mm)	Abdomen Circum. (mm)	λm	λk	λL	λp	APTS (Bar)
Ramachandra et al. 2016	04_1	PMHS04	M	80	86	184	25.4	3	185		1.132	1.459	1.051	1.421	2.578341
	06	PMHS06	M	25	74	178	23.4	2	173		0.974	1.561	1.017	1.275	2.31459
	07_1	PMHS07	M	48	67	174	22.1	3	225		0.882	1.200	0.994	1.017	1.845381
Guettler et al. 2023*	V13-4	SM129	M	79	63	178	19.9	4	230		0.829	1.175	1.017	1.021	2.647907
	V13-5	SM155	M	65	85	168	30.1	4	294		1.118	0.917	0.960	0.933	2.421047
	V13-6	SM161	M	83	81	175	26.4	5	271		1.066	0.996	1.000	1.030	2.671508
	V14-5	SN156	M	68	89	188	25.2	2	263		1.171	1.026	1.074	1.265	3.678796
	V14-6	SM157	M	59	68	173	22.7	3	248		0.895	1.090	0.989	0.965	2.806925
	V14-7	SM160	M	74	79	178	24.9	3	262		1.039	1.032	1.017	1.071	3.116297
	V15-5	SM152	M	63	81	180	25.0	2	262		1.066	1.030	1.029	1.109	3.625025
	V15-6	SM153	M	51	64	168	22.7	4	247		0.842	1.091	0.960	0.883	2.888847
	V15-7	SM165	M	51	89	175	29.1	4	288		1.171	0.939	1.000	1.048	3.428116
	V19-5	SM154	M	74	89	178	28.1	0	282		1.171	0.959	1.017	1.096	4.216714
	V19-6	SM095	M	74	64	170	22.1	3	244		0.842	1.106	0.971	0.911	3.503009
	V19-7	SM159	M	29	73	163	27.5	3	278		0.961	0.972	0.931	0.838	3.224652

*The abdomen depth and circumference were not reported. The abdomen depth in the table were generated with linear regression as described in the abdomen section.

Table A5 THOR-AV A.S.I.S. load cell output (unscaled)

References	Submarining	Left Fx (N)	Right Fx (N)	Total Fx (N)	Test or FE
Luet et al. 2006, Config1	No	-307	-152.5	-460	FE
Luet et al. 2006, Config2	Yes	-1115	-563.4	-1599	FE
Luet et al. 2006, Config3	Yes	-478	-272.3	-735	FE
Uriot et al. 2015, Rear	Yes	2301	-2155.4	-4456	Test
Uriot et al. 2015, Front	No	1828	-1838.8	-3663	Test
Richardson et al. 2020a	No	3701	-3508.1	-7017	Test
UMTRI, 32 km/h, 25°	No	92	-276.5	-362	Test
UMTRI, 32 km/h, 45°	No	109	-482.4	-585	Test
UMTRI, 52 km/h, 25°	No	-3957	-3021.7	-6971	Test
UMTRI, 52 km/h, 45°	No	-3884	-2849.8	-6620	Test

Baudrit 2022 Stapp	No	-1254	-810.7	-1948	FE
Guettler et al. 2023 (V13)	Yes	3874	-3173	-6987	Test
Guettler et al. 2023 (V14)	Moderate	2118	-997	-2537	Test
Guettler et al. 2023 (V15)	Moderate	5020	-1145	-5681	Test
Guettler et al. 2023 (V19)	No	4151	-1302	-4882	Test

Table A6. PMHS load cases and THOR-AV ASIS force scaled to the respective PMHS specimen

References	Test #	Specimen #	Sex	Age	Mass (kg)	Stature (cm)	AIS	λm	λstature	λm*λstature	Max Fx (N)	Tota Fx (N)
Luet et al. 2012	Config 1	631	M	67	59.5	171.5	2	0.783	0.980	0.876	-241	-360
	Config 1	632	M	85	69.5	167	0	0.914	0.954	0.873	-281	-420
	Config 1	633	M	76	54	163	2	0.711	0.931	0.662	-218	-327
	Config 2	634	M	68	79	170	2	1.039	0.971	1.010	-1159	-1662
	Config 2	636	M	77	61.5	171	0	0.809	0.977	0.791	-902	-1294
	Config 3	637	M	79	57	161.5	2	0.750	0.923	0.692	-358	-551
	Config 3	638	M	67	58	170.5	2	0.763	0.974	0.744	-365	-561
	Config 3	639	M	90	71	162	0	0.934	0.926	0.865	-446	-687
Uriot et al. 2015 (rear seat)	SubBIO_22	683	M	55	92	177	2	1.211	1.011	1.224	-2786	-5394
	SubBIO_23	679	M	86	67	168	2	0.882	0.960	0.846	-2029	-3928
	SubBIO_24	681	M	87	77	175	2	1.013	1.000	1.013	-2332	-4514
	SubBIO_25	682	M	87	64	171	2	0.842	0.977	0.823	-1938	-3752
Uriot et al. 2015 (front seat)	SubBIO_26	678	M	85	79	165	0	1.039	0.943	0.980	-1911	-3807
	SubBIO_27	677	M	84	57	170	0	0.750	0.971	0.729	-1379	-2747
	SubBIO_28	676	M	84	64	170	0	0.842	0.971	0.818	-1548	-3085
	SubBIO_29	680	M	89	77	175	0	1.013	1.000	1.013	-1863	-3711
Richardson et al. 2020a	529	930	M	66	74	175	2	0.974	1.000	0.974	-3603	-6832
	530	630	M	53	57	175	2	0.750	1.000	0.750	-2776	-5263
	531	901	M	72	74	185	2	0.974	1.057	1.029	-3603	-6832
	532	662	M	25	75	174	0	0.987	0.994	0.981	-3652	-6924
	533	815	M	55	74	180	2	0.974	1.029	1.002	-3603	-6832
	b12796/AV2003	F201281	M	72	64.4	174.2	0	0.847	0.995	0.843	-234	-306

References	Test #	Specimen #	Sex	Age	Mass (kg)	Stature (cm)	AIS	λm	λstature	λm*λstature	Max Fx (N)	Tota Fx (N)
UMTRI 32 km/h, 25°	b13109/AV2104	WSU702	M	80	80.28	170.1	0	1.056	0.972	1.027	-292	-382
	b13124/AV2107	S210739	M	70	63.72	175.65	0	0.838	1.004	0.842	-232	-303
UMTRI 32 km/h, 45°	b12795/AV2002	35764	M	91	76.1	174.9	0	1.001	0.999	1.001	-483	-586
	b13110/AV2105	WSU711	M	85	71.1	169.7	0	0.936	0.970	0.907	-451	-547
	b13119/AV2106	WSU705	M	71	53	166.3	0	0.697	0.950	0.663	-336	-408
UMTRI 50 km/h,	b13196/AV2211	WSU039	M	71	76.1	174.3	3	1.001	0.996	0.997	-3962	-6981
UMTRI 50 km/h, 45°	b13193/AV2208	C220039	M	62	60.8	173.9	3	0.800	0.994	0.795	-3107	-5296
	b13194/AV2209	I220401	M	58	65.8	176.1	4	0.866	1.006	0.871	-3363	-5732
	b13195/AV2210	WSU037	M	63	82	172.2	3	1.079	0.984	1.062	-4191	-7143
Baudrit et al. 2022	1	746	M	73	69	167	3	0.908	0.954	0.866	-1138	-1769
	2	744	M	88	76	169	1	1.000	0.966	0.966	-1254	-1948
	3	745	M	90	84	160	4	1.105	0.914	1.011	-1386	-2153
Guettler et al. 2023	V13-4	SM129	M	79	63	178	0	0.829	1.017	0.843	-3211	-5791
	V13-5	SM155	M	65	85	168	0	1.118	0.960	1.074	-4333	-7814
	V13-6	SM161	M	83	81	175	0	1.066	1.000	1.066	-4129	-7446
	V14-5	SN156	M	68	89	188	2	1.171	1.074	1.258	-2480	-2971
	V14-6	SM157	M	59	68	173	0	0.895	0.989	0.885	-1895	-2270
	V14-7	SM160	M	74	79	178	0	1.039	1.017	1.057	-2202	-2637
	V15-5	SM152	M	63	81	180	3	1.066	1.029	1.096	-5351	-6054
	V15-6	SM153	M	51	64	168	0	0.842	0.960	0.808	-4228	-4784
	V15-7	SM165	M	51	89	175	2	1.171	1.000	1.171	-5879	-6652
	V19-5	SM154	M	74	89	178	2	1.171	1.017	1.191	-4861	-5717
	V19-6	SM095	M	74	64	170	0	0.842	0.971	0.818	-3495	-4111
	V19-7	SM159	M	29	73	163	0	0.961	0.931	0.895	-3987	-4689

APPENDIX 2

THOR-AV FE model (v0.7.2) were validated against a series of physical test data. The peak values for the validation tests were summarized below for the readers' reference.

Lumbar Spine

An isolated lumbar spine test was designed to validate the lumbar spine by itself. The isolated lumbar spine was mounted on a sled frame and a rigid body mass was mounted on top of the spine to remove all other contributing factors. The test setup is shown in Figure A1. The sled speeds of 4 m/s and 6.4 m/s were used in each test configuration.

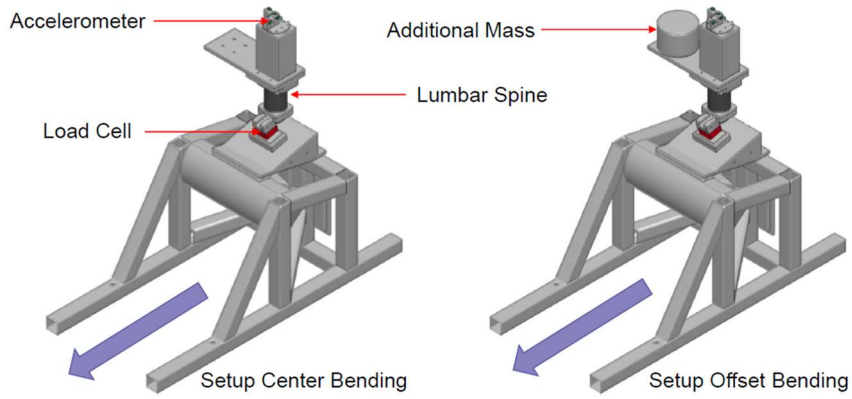

Figure A1. Isolated lumbar spine test setup for FE model validation, left – center bending, right – offset bending)

Table A7 Isolated lumbar spine validation - T12 load cell peak values (center bending 4 m/s)

Test #	T12 Fx (N)	T12 Fz (N)	T12 My (Nm)
Test1	-747	596	223
Test2	-756	612	225
Average	-752	604	224
FE	-678	485	214
Difference	-10%	-20%	-4%

Table A8. Isolated lumbar spine FE validation - T12 load cell peak values (center bending 6.4 m/s)

Test #	T12 Fx (N)	T12 Fz (N)	T12 My (Nm)
Test1	-1148	1029	331.376
Test2	-1141	1058	330.080
Test3	-1148	1062	330.969
Average	-1146	1050	331
FE	-1149	965	348
Difference	0.3%	-8.1%	5.2%

Table A9. Isolated lumbar spine FE validation - T12 load cell peak values (offset bending, 4 m/s)

	T12 Fx (N)	T12 Fz (N)	T12 My (Nm)	T12 Mz (Nm)
	-820	488	222	-104
	-821	480	221	-105
	-821	478	221	-106
	-702	485	236	-99

Table A10 Isolated lumbar spine FE validation - T12 load cell peak values (offset bending, 6.4 m/s)

Test #	T12 Fx (N)	T12 Fz (N)	T12 My (Nm)	T12 Mz (Nm)
Test1	-1365	714	351	-168
Test2	-1348	702	348	-168
Test3	-1352	713	347	-168
Average	-1355	710	349	-168
FE	-1443	909	392	-172
Difference	6.5%	28.1%	12.5%	2.3%

Richardson et al. 2020 Test Condition

The THOR-AV FE model was validated in Richardson et al. 2020 test condition, which is a sled test on a semi-rigid seat, with torso angle at 45 degrees at 50 km/h impact speed. The peak values of the ASIS forces are summarized in Table A11 and A12.

Table A 11. Lumbar validation in Richardson et al. 2020a test condition

Test #	T12 Fx (N)	T12 Fz (N)	T12 My (Nm)
Test1	501	-4754	260
Test2	473	-4989	271
Test3	428	-4919	287
Average	467	-4887	273
FE	438	-4892	351
Difference	-6.3%	0.1%	28.7%

Table A12 ASIS force validation in Richardson et al. 2020a test condition.

Test #	Left ASIS Fx (N)	Right ASIS Fx (N)
Test1	3719	3460
Test2	3735	3394
Test3	3648	3670
Average	3701	3508
FE	4123	3394
Difference	11.4%	-3.2%

Isolated APTS pendulum validation tests

Isolated APTS pendulum validation tests were conducted with two speeds, 0.74 m/s and 1.13 m/s. The test setup is shown in the

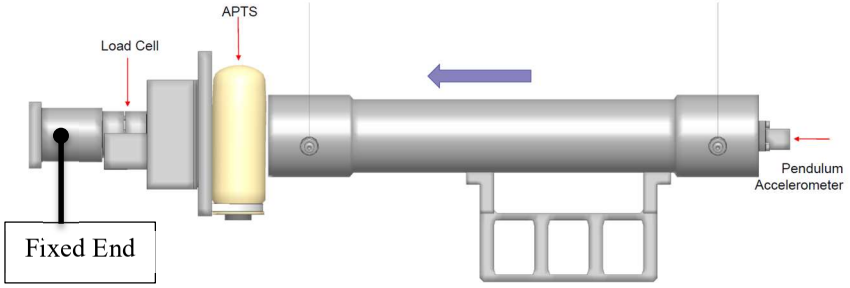

Figure A2. Isolated APTS pendulum validation test setup

Table A13 Isolated APTS validation results at 0.74 m/s impact speed

Test #	APTS Pressure (kPa)	Load Cell Force (N)	Probe Ax (g)
Test1	123.0	590	5.0
Test2	119.4	595	5.0
Test3	120.1	596	5.1
Average	120.8	594	5.0
FE	120.2	560	4.7
Difference	-0.5%	-5.7%	-7.0%

Table A14 Isolated APTS validation results at 1.13 m/s impact speed

Test #	APTS Pressure (kPa)	Load Cell Force (N)	Probe Ax (g)
Test1	200.2	1114	9.5
Test2	200.1	1115	9.4
Test3	197.9	1114	9.5
Average	199.4	1114	9.5
FE	200.1	1119	9.5
Difference	0.4%	0.5%	0.2%

Pelvis Pendulum Test

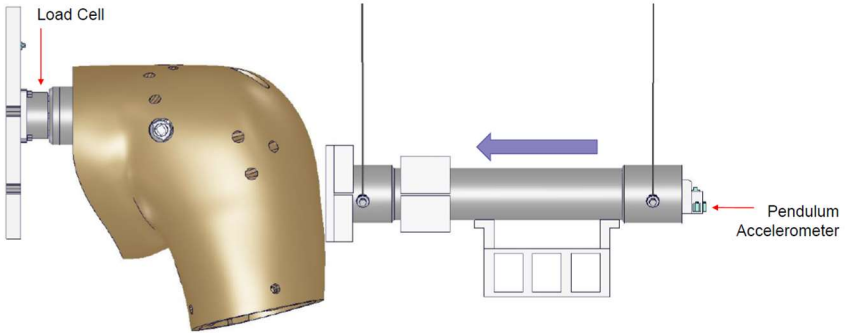

Figure A3. Pelvis pendulum test at 2.0 m/s

Table A 15. Peak values of pelvis pendulum impact test at 2.0 m/s

Test	Pelvis Fx (N)	Pelvis Fz (N)	Pelvis My (Nm)	Pendulum Force (N)
test 1	-525	2265	193	2030
test 2	-484	2168	185	1955
test 3	-441	2005	163	1800
Average	-483	2146	180	1928
FE	-389	2257	197	1850
Difference	-24.3%	4.9%	8.5%	-4.2%